Part II
Robustness and Fragility

Chapter 8
Cascading Failures in Interdependent Economic Networks

Shlomo Havlin and Dror Y. Kenett

Abstract Throughout the past decade, there has been a significant advance in understanding the structure and function of networks, and mathematical models of networks are now widely used to describe a broad range of complex systems, such as socio-economic systems. However, the significant majority of methods have dealt almost exclusively with individual networks treated as isolated systems. In reality an individual network is often just one component in a much larger complex multi-level network (network of networks, NON). The NON framework provides critical new insights into the structure and function of real-world complex systems. One such insight is that NON system is significantly more vulnerable to shocks and damages, which has lead to the development of the theory of cascading failures in interdependent networks. Here we provide an overview of this theory, and one example of its application to economic systems.

8.1 Introduction

The growth of technology, globalization, and urbanization has caused world-wide human social and economic activities to become increasingly interdependent [1–13]. From the recent financial crisis it is clear that components of this complex system have become increasingly susceptible to collapse. Current models have been unable to predict instability, provide scenarios for future stability, or control or even mitigate systemic failure. Thus, there is a need of new ways of quantifying complex system vulnerabilities as well as new strategies for mitigating systemic damage and increasing system resiliency [14, 15]. Achieving this would also provide new insight into such key issues as financial contagion [16, 17] and systemic risk [18–20] and would provide a way of maintaining economic and financial stability in the future.

S. Havlin (✉)
Department of Physics, Bar-Ilan University, Ramar Gan, Israel
e-mail: havlins@gmail.com

D.Y. Kenett (✉)
Center for Polymer Studies and Department of Physics, Boston University, MA, USA
e-mail: drorkenett@gmail.com

H. Takayasu et al. (eds.), *Proceedings of the International Conference on Social Modeling and Simulation, plus Econophysics Colloquium 2014*, Springer
Proceedings in Complexity, DOI 10.1007/978-3-319-20591-5_8

Throughout the past decade, there has been a significant advance in understanding the structure and function of networks, and mathematical models of networks are now widely used to describe a broad range of complex systems, from techno-social systems to interactions amongst proteins [21–32]. However, the significant majority of methods have dealt almost exclusively with individual networks treated as isolated systems. In reality an individual network is often just one component in a much larger complex multi-level network (network of networks). As technology has advanced, the coupling between networks is becoming stronger and stronger. For example, there is a strong coupling between human mobility (which can be tracked by mobile networks) and transport networks. In these interdependent networks, the failures of nodes in one network will cause failures of dependent nodes in other networks, and vice-versa [33–41]. This process happens recursively, and leads to a cascade of failures in the network of networks system. As in physics, when only the individual particles were studied it was made possible to understand the properties of gas; however, when the transition was made to study the interactions between these particles, it was finally made possible to understand and describe liquids and solids, as well as the concept of phase transitions. Such a development in network science has led to a significant paradigm shift, which has opened the door to the understanding of a multitude of new features and phenomena (see schematic overview in Fig. 8.1). Here we will review the theory of cascading failures in interdependent networks, and present one application in economic networks.

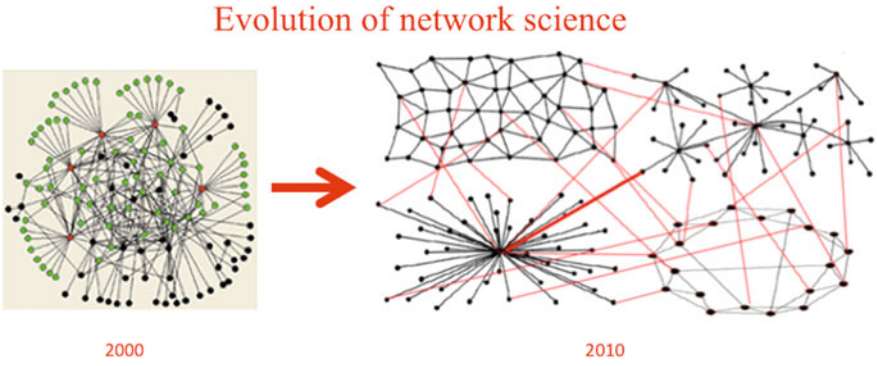

Fig. 8.1 Schematic representation of the scope of network science research from the beginning of the twenty first century, from focusing on the case of a single network, to the case of interconnected and interdependent networks. The *black links* represent connectivity links while the *red links* are dependency links. The concept of dependency links and the generalization of percolation theory to include such links was first introduced in Buldyrev et al. [33]

8.2 Overview of Cascading Failure Processes in Interdependent Networks

The theory for cascading failures in interdependent networks was introduced in [33, 34, 36, 37, 42, 43], and we review it shortly in this section. In order to model interdependent networks, consider two networks, A and B, in which the functionality of a node in network A is dependent upon the functionality of one or more nodes in network B (see Fig. 8.2), and vice-versa: the functionality of a node in network B is dependent upon the functionality of one or more nodes in network A. The networks can be interconnected in several ways. In the most general case we specify a number of links that arbitrarily connect pairs of nodes across networks A and B. The direction of a link specifies the dependency of the nodes it connects, i.e., link $A_i \rightarrow B_j$ provides a critical resource from node A_i to node B_j. If node A_i stops functioning due to attack or failure, node B_j stops functioning as well but not vice-versa. Analogously, link $B_i \rightarrow A_j$ provides a critical resource from node B_i to node A_j.

To study the robustness of interdependent networks systems, we begin by removing a fraction $1-p$ of network A nodes and all the A-edges connected to these nodes. As an outcome, all the nodes in network B that are connected to the removed A-nodes by $A \rightarrow B$ links are also removed since they depend on the removed nodes in network A. Their B edges are also removed. Further, the removed B nodes will cause the removal of additional nodes in network A which are connected to the removed B-nodes by $B \rightarrow A$ links. As a result, a cascade of failures that eliminates virtually all nodes in both networks can occur. As nodes and edges are removed, each network breaks up into connected components (clusters). The clusters in network A (connected by A-edges) and the clusters in network B (connected by B-edges) are different since the networks are each connected differently. If one assumes that small clusters (whose size is below certain threshold) become non-functional, this may invoke a recursive process of failures that we now formally describe.

The insight based on percolation theory is that when the network is fragmented the nodes belonging to the giant component connecting a finite fraction of the network are still functional, but the nodes that are part of the remaining small

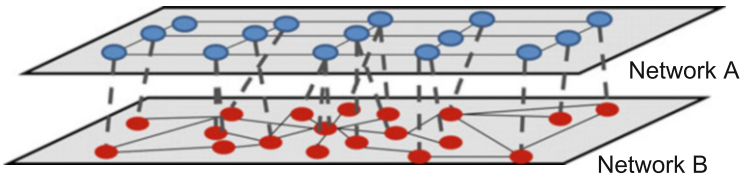

Fig. 8.2 Example of two interdependent networks. Nodes in network B (e.g. communications network) are dependent on nodes in network A (e.g. power grid) for power; nodes in network A are dependent on network B for control information

clusters become non-functional. Thus in interdependent networks only the giant mutually-connected cluster is of interest. Unlike clusters in regular percolation whose size distribution is a power law with a p-dependent cutoff, at the final stage of the cascading failure process just described only a large number of small mutual clusters and one giant mutual cluster are evident. This is the case because the probability that two nodes that are connected by an A-link and their corresponding two nodes are also connected by a B-link scales as $1/N_B$, where N_B is the number of nodes in network B. So the centrality of the giant mutually-connected cluster emerges naturally and the mutual giant component plays a prominent role in the functioning of interdependent networks. When it exists, the networks preserve their functionality, and when it does not exist, the networks split into fragments so small they cannot function on their own. In Fig. 8.3 we present a schematic representation of an example of a tree-like network of networks, composed of five networks. The cascading failure process is applied by removing $1-p$ nodes, and calculating the size of the mutual giant component, P_∞. We present (Fig. 8.2) a comparison between P_∞ of $n = 1, 2, 5$ networks, and show that the network of networks system is more vulnerable to cascading failures. Finally, we show (Fig. 8.2) the analytical

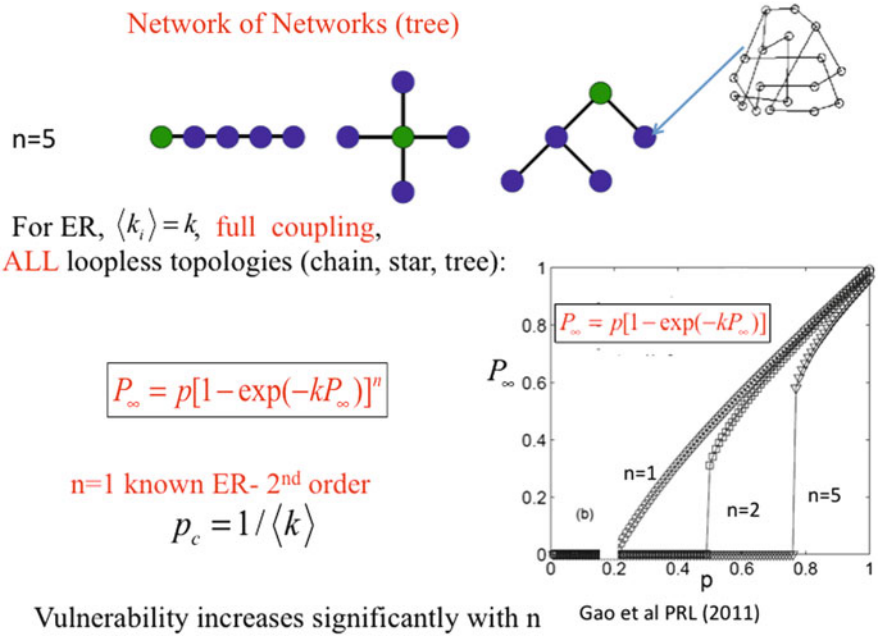

Fig. 8.3 Schematic representation of an example of a tree-like network of networks, composed of 5 networks. The cascading failure process is applied by removing a fraction $1 - p$ nodes, and calculating the size of the mutual giant component, P_∞. We present a comparison between P_∞ of $n = 1, 2, 5$ networks, and show that the network of networks system is more vulnerable to cascading failures. Finally, we show the analytical relationship between P_∞, n, k and p, which for the case of one network collapses to the well known ER formalism

relationship between P_∞, n, k and p, which for the case of a single network ($n = 1$) collapses to the well known ER formalism [24].

8.3 Cascading Failures in Economic Networks

Network science has greatly evolved in the twenty first century, and is currently a leading scientific field in the description of complex systems, which affects every aspect of our daily life [2, 22–25]. Network theory provides the means to model the functional structure of different spheres of interest, and thus, understanding more accurately the functioning of the network of relationships between the actors of the system, its dynamics and the scope or degree of influence. In addition, it measures systemic qualities, e.g., the robustness of the system to specific scenarios, or the impact of policy on system actions. The advantage offered by the network science approach is that instead of assuming the behavior of the agents of the system, it rises empirically from the relationships that they really hold; hence, the resulting structures are not biased by theoretical perspectives or normative approaches imposed 'by the eye of the researcher'. On the contrary, the modeling by network theory could validate behavioral assumptions by economic theories. Network theory can be of interest to various edges of the financial world: the description of systemic structure, analysis and evaluation of contagion effects, resilience of the financial system, flow of information, and the study of different policy and regulation scenarios, to name a few [44–57]. Once the network structure and topology is uncovered, it is possible to test many features of the economic system. One critical issue is the resilience of economic and financial systems to shock scenarios, which is commonly investigated using stress tests [58–61]. Cascading failure processes can be applied to study the stability of economic and financial systems, and uncover global and local vulnerabilities to the system. Here, we review a recent application of the theory of cascading failures in interdependent economic systems to quantify and rank the economic influence of specific industries and countries, which was recently introduced by Li et al. [51].

Li et al [51] have examined the interdependent nature of economies between and within 14 countries and the rest of the world (ROW), using input-output table [62] during the period 1995–2011. The economic activity in each country is divided into 35 industrial classifications. Each cell in the table shows the output composition of each industry to all other 525 industries and its final demand and export to the rest of the world (see [63]). From the IO table, an output network is constructed using the 525 industries as nodes and the output product values as weighted links based on the input-output table. The goal of this work is to introduce a methodology for quantifying the importance of a given industry in a given country to global economic stability with respect to other industries in countries that are related to this industry. The authors use the theory of cascading failures in interdependent networks to gain valuable information on the local and global influence on global stability of different economic industries.

In order to identify and rank the influence of industries in the stability of this global network, the authors perform a cascading failure tolerance analysis [33, 51]. The model can be described as follows. Suppose industry A fails, other industries can no longer sell their products to industry A and thus they lose that revenue. The revenue of each industry is reduced by a fraction p', which for each industry is defined as the revenue reduction caused by the failure of industry A divided by that industry's total revenue. The tolerance fraction ϕ is the threshold above which an industry fails. This occurs when reduced revenue fraction p' is larger than tolerance fraction ϕ. Here we assume that (i) ϕ is the same for all industries and that every industry fails when its $p' > \phi$ and (ii) the failure of an industry in country A does not reduce the revenue of the other industries in the same country A because they are able to quickly adjust to the change. The methodology can be schematically illustrated as follows (see Fig. 8.4): In step 1, industry A in country i fails. This causes other industries in other countries to fail if their $p' > \phi$. Assume that in step 2 industries B, C, and D fail. The failure of these industries in step 2 will reduce other industries' revenue and cause more industries including those in country i to have a reduced fraction p'. Thus in step 3 there is an increased number of industries whose $p' > \phi$. Eventually the system reaches a steady state in which no more industries

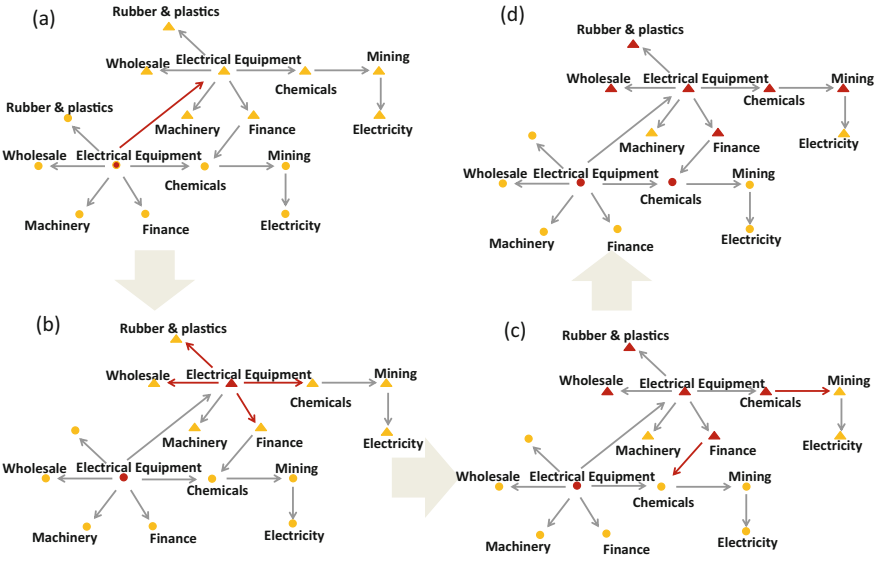

Fig. 8.4 Schematic representation of each step in the cascading failure propagation in the world economic network (**a**⟶**b**⟶**c**⟶**d**). We present an example of two countries, where *circle* nodes represent country 1, and *triangles* represent country 2. Both countries have the same industries, and the *arrow* between two nodes points in the direction of money flow. The different subpanels demonstrate the cascade of the damage, after an initial failure in electrical equipment industry in Country 1 (*circle*) which causes a failure of electrical equipment industry in Country 2, which cascades into other industries. After [51]

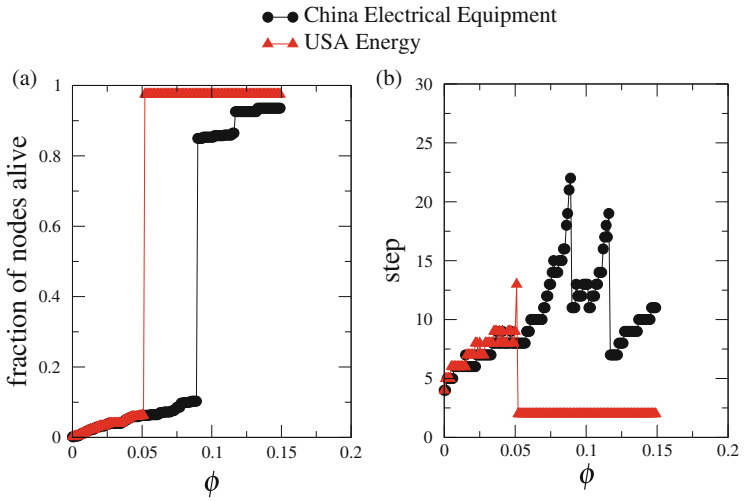

Fig. 8.5 Typical examples of industry tolerance threshold ϕ_c. (**a**)(*left*) the *black curve* shows the fraction of surviving industries as a function of tolerance threshold for the case when the electrical equipment industry in China fails in year 2009 and the *red curve* represents the case of the failure of the energy industry in 2009 in the USA. (**b**)(*right*) Number of failure steps as a function of p. The total number of steps is the number of cascades it takes for the network to reach a steady state after certain initial failure. After [51]

fail. The surviving industries will all have a reduced revenue fraction that is smaller than the tolerance fraction, i.e., $p' \leq \phi$.

Figure 8.5 shows an example of the failures of electric equipment industry in China and the energy industry in the US for the 2009 WIOT and shows the fraction of the largest cluster of connected industries as a function of the tolerance fraction ϕ after the Chinese electric equipment industry becomes malfunction and is removed from the network due to a large shock to the industry. The shock could result from different causes, such as natural environmental disaster, government policy changes, insufficient financial capability. The removal of China electric equipment industry will cause revenue reduction in other industries because China electric equipment industry is not able to buy products and provide money to other industries. When ϕ is small, the industries are fragile and sensitive to the revenue reduction, causing most of the industries fail, and the number of the surviving industries is very small. When ϕ is large, the industries can tolerate large revenue reduction and are more robust when revenue decreases. The number of the surviving industries tends to increase abruptly at a certain $\phi = \phi_c$ value as ϕ increases. Figure 8.5b shows the number of steps that elapse before a stable state is reached as a function of tolerance fraction ϕ after removing the Chinese electric equipment industry or the US energy industry. The number of steps reaches a peak when ϕ approaches criticality ϕ_c [64].

Finally, Li et al. [51] use the cascading failure methodology to rank the economic importance of individual countries, and track how it evolves in time. Figure 8.6 (left)

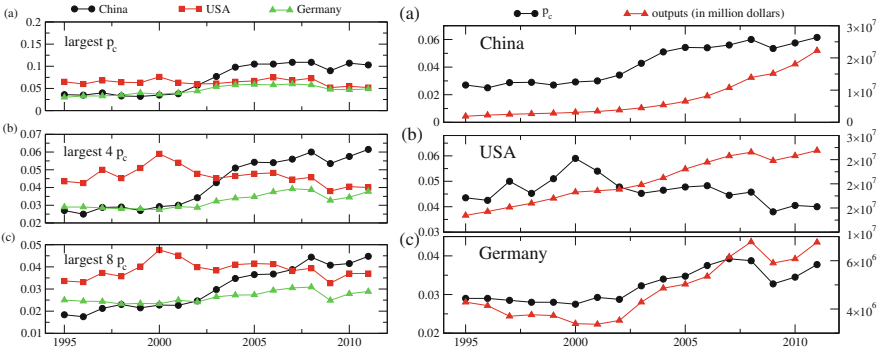

Fig. 8.6 (*left*) Tolerance ϕ_c changes of China, the USA and Germany for 17 years: *top*—the largest tolerance ϕ_c; *middle*—the average of 4 largest ϕ_c; and *bottom*—the average of 8 largest p_c in each country. These results show that the economic importance of China is increasing, while that of the USA is decreasing. (*right*) Tolerance ϕ_c of China, the USA and Germany comparing to the total product output value. For each country, the ϕ_c is an average of the largest four industry ϕ_c of this country (*black circles*). The product output (*red triangle*) value is the money flow a country supplies to the rest of the countries, which also indicates its impact to foreign countries. After [51]

shows the average of ϕ_c of country for the 17-year period investigated, for the case of China, USA and Germany: top—the largest tolerance ϕ_c; middle—the average of four largest industries ϕ_c; and bottom—the average of 8 largest ϕ_c in each country. The results of Li et al [51] present how the economic importance of China relative to that of the USA shows a consistent increase from year to year, illustrating how the economic power structure in the world's economy has been changing during time. Finally, to further validate these results, the total product output (see Fig. 8.6 (right), red triangles) and average tolerance ϕ_c (see Fig. 8.6 (right), black circles) for China, USA, and Germany, as a function of time. The product output value is the total money flow a country supplies to the other countries plus value added in the products, which also indicates its total trade impact on foreign countries.

8.4 Summary

In summary, this paper presents a review of the recently-introduced mathematical framework of for cascading failures in a Network of Networks (NON), particularly in economic NON. In interacting networks, when a node in one network fails it usually causes dependent nodes in other networks to fail which, in turn, may cause further damage in the first network and result in a cascade of failures with catastrophic consequences. This analytical framework enables to follow the dynamic process of the cascading failures step-by-step and to derive steady state solutions [65–67]. This formalism provides critical new information on the resilience and vulnerabilities of real world complex systems, such as economic and financial

systems. In economics, some key applications include new stress test tools, such as those presented by Li et al. [51] and Levy-Carciente et al. [61]. Furthermore, these developed tools can be used to introduce intervention strategies in order to manage and mitigate once a cascade of failures is set off in the system (see for example [68]).

Acknowledgements We acknowledge financial support from Office of Naval Research (ONR), DTRA, BSF, the LINC (No. 289447) and the Multiplex (No. 317532) EU projects, the DFG, and the Israel Science Foundation.

References

1. Helbing D, Balietti S (2010) arXiv preprint arXiv:1012.4446
2. Havlin S, Kenett D, Ben-Jacob E, Bunde A, Cohen R, Hermann H, Kantelhardt J, Kertész J, Kirkpatrick S, Kurths J, et al (2012) Eur Phys J Spec Top 214(1):273
3. San Miguel M, Johnson JH, Kertesz J, Kaski K, Díaz-Guilera A, MacKay RS, Loreto V, Érdi P, Helbing D (2012) Eur Phys J Spec Top 214(1):245
4. Helbing D (ed) (2012) Social self-organization. Springer, Berlin, pp 261–284
5. Lazer D, Pentland AS, Adamic L, Aral S, Barabasi AL, Brewer D, Christakis N, Contractor N, Fowler J, Gutmann M, et al (2009) Science 323(5915):721. (New York, NY)
6. King G (2011) Science(Washington) 331(6018):719
7. Lorenz J, Rauhut H, Schweitzer F, Helbing D (2011) Proc Natl Acad Sci 108(22):9020
8. Yamasaki K, Fujiwara T, Yoshizawa K, Miyake S, Zheng Z, Gao X, Sakurai N (2012) Proceedings of international conference on business management & IS, pp 130–140
9. Meng B, Inomata S (2009) Production networks and spatial economic interdependence: An international input-output analysis of the asia-pacific region. Technical report. Institute of Developing Economies, Japan External Trade Organization (JETRO)
10. Rinaldi SM, Peerenboom JP, Kelly TK (2001) IEEE Control Syst 21(6):11
11. Solomon S, Levy M (2003) Quant Finan 3(1):c12
12. Levy M (2010) Phys A Stat Mech Appl 389(21):4913
13. Klimek P, Hausmann R, Thurner S (2012) PloS one 7(6):e38924
14. Farmer JD, Foley D (2009) Nature 460(7256):685
15. Lux T, Westerhoff F (2009) Nat Phys **5**(1):2
16. Forbes K, Rigobon R (2001) International financial contagion. Springer, New York, pp 43–66
17. Forbes KJ, Rigobon R (2002) J Financ 57(5):2223
18. Bodie Z, Kane A, Marcus AJ (2002) Investments (Tang Kinh Cac, 2002)
19. Billio M, Getmansky M, Lo AW, Pelizzon L (2010) Econometric measures of systemic risk in the finance and insurance sectors. Techniacl report, National Bureau of Economic Research
20. Bisias D, Flood M, Lo AW, Valavanis S (2012) Annu Rev Financ Econ 4(1):255
21. Albert R, Barabási AL (2002) Rev Mod Phys 74(1):47
22. Newman MEJ Networks: an introduction (OUP, 2009)
23. Jackson MO (2010) Social and economic networks. Princeton University Press, Princeton
24. Boccaletti S, Latora V, Moreno Y, Chavez M, Hwang DU (2006) Phys Rep 424(4):175

25. Cohen R, Havlin S 2010 Complex networks: structure, robustness and function. Cambridge University Press, Cambridge
26. May RM (2013) Philos Trans R Soc A Math Phys Eng Sci 371(1987):20120376
27. Bashan A, Bartsch RP, Kantelhardt JW, Havlin S, Ivanov PC (2012) Nat Commun 3:702
28. Barrat A, Barthelemy M, Vespignani A (2008) Dynamical processes on complex networks. Cambridge University Press, Cambridge
29. Vespignani A (2010) Nature 464(7291):984
30. Lux T (2011) Nature 469(7330):303
31. Li D, Fu B, Wang Y, Lu G, Berezin Y, Stanley HE, Havlin S (2015) Proc Natl Acad Sci 112(3):669
32. Ludescher J, Gozolchiani A, Bogachev MI, Bunde A, Havlin S, Schellnhuber HJ (2014) Proc Natl Acad Sci 111(6):2064
33. Buldyrev SV, Parshani R, Paul G, Stanley HE, Havlin S (2010) Nature 464(7291):1025
34. Parshani R, Buldyrev SV, Havlin S (2010) Phys Rev Lett 105(4): 048701
35. Bashan A, Berezin Y, Buldyrev SV, Havlin S (2013) Nat Phys 9(10):667
36. Gao J, Buldyrev SV, Stanley HE, Havlin S (2012) Nat Phys 8(1):40
37. Kenett DY, Gao J, Huang X, Shao S, Vodenska I, Buldyrev SV, Paul G, Stanley HE, Havlin S (2014) Networks of networks: the last frontier of complexity Springer, New York, pp 3–36
38. Boccaletti S, Bianconi G, Criado R, Del Genio C, Gómez-Gardeñes J Romance M, Sendina-Nadal I, Wang Z, Zanin M (2014) Phys Rep 544(1):1
39. Lee KM, Kim JY, Cho Wk, Goh K, Kim I (2012) New J Phys 14(3):033027
40. Baxter G, Dorogovtsev S, Goltsev A, Mendes J (2012) Phys Rev Lett 109(24):248701
41. Peixoto TP, Bornholdt S (2012) Phys Rev Lett 109(11):118703
42. Havlin S, Kenett D, Bashan A, Gao J, Stanley H (2014) Eur Phys J Spec Top 223(11):2087
43. Havlin S, Stanley HE, Bashan A, Gao J, Kenett DY (2014) Chaos, Solitons Fractals
44. Lillo F (2010) Encyclopedia of life support systems (EOLSS), Developed under the auspices of the UNESCO
45. Summer M (2013) Annu Rev Financ Econ 5(1):277
46. Tumminello M, Lillo F, Mantegna RN (2010) J Econ Behav Organ 75(1):40
47. Kenett DY, Tumminello M, Madi A, Gur-Gershgoren G, Mantegna R, Ben-Jacob E (2010) PloS one 5(12):e15032
48. Kenett DY, Raddant M, Lux T, Ben-Jacob E (2012) PloS one 7(2):e31144
49. Cont R (2013) Handbook on systemic risk. Cambridge University Press, Cambridge, p 285
50. Glasserman P, Young HP (2015) How likely is contagion in financial networks? J Bank Financ 50:383–399
51. Li W, Kenett DY, Yamasaki K, Stanley HE, Havlin S (2014) arXiv preprint arXiv:1408.0443
52. Garas A, Argyrakis P, Rozenblat C, Tomassini M, Havlin S (2010) New J Phys 12(11):113043
53. Haldane AG, May RM (2011) Nature 469(7330):351
54. Haldane AG, et al. (2009) Speech delivered at the financial student association, Amsterdam, April
55. Cont R, Moussa A, Bastos E (2010) e Santos. Available at SSRN:1733528
56. Amini H, Cont R, Minca A (2012) Stress testing the resilience of financial networks. Int J Theor Appl Financ 15(01):1250006
57. Chan-Lau J, Espinosa M, Giesecke K, Solé J (2009) IMF global financial stability report, vol. 2
58. Boss M, Elsinger H, Summer M, Thurner S (2004) Quant Finan 4(6):677
59. Langfield S, Liu Z, Ota T (2012) Financial sevices authority
60. Martínez Jaramillo S, Kabadjova B, Bravo Benítez B, Solórzano J (2012) Margain, Systemic risk analysis by means of network theory: An empirical study of the mexican banking system. Technical report Banco de México working papers
61. Levy Carciente S, Kenett DY, Avakian A, Stanley HE, Havlin S (2014) Available at SSRN 2482742
62. Timmer M, Erumban A, Gouma R, Los B, Temurshoev U, de Vries G, Arto I (2012) WIOD Background document available at www.wiod.org

63. World Input Output Database (2012) www.wiod.org
64. Parshani R, Buldyrev SV, Havlin S (2011) Proc Natl Acad Sci 108(3):1007
65. Gao J, Buldyrev S, Havlin S, Stanley H (2012) Phys Rev E 85(6):066134
66. Zhou D, Bashan A, Cohen R, Berezin Y, Shnerb N, Havlin S (2014) Phys Rev E 90(1):012803
67. Dong G, Gao J, Du R, Tian L, Stanley H.E, Havlin S (2013) Phys Rev E 87(5):052804
68. Majdandzic A, Podobnik B, Buldyrev SV, Kenett DY, Havlin S, Stanley HE Nat Phys 10(1):34 (2014)

Chapter 9
Do Connections Make Systems Robust? A New Scenario for the Complexity-Stability Relation

Takashi Shimada, Yohsuke Murase, and Nobuyasu Ito

Abstract Whether interactions among the elements make the system robust or fragile has been a central issue in broad range of field. Here we introduce a novel type of mechanism which governs the robustness of open and dynamical systems such as social and economical systems, based on a very simple mathematical model. This mechanism suggest a moderate number (~ 10) of interactions per element is optimal to make the system against successive and unpredictable disturbances. The relation between this very simple model and more detailed nonlinear dynamical models is discussed, to emphasize the relevance of this newly reported mechanism to the real phenomena.

9.1 Introduction

Most real complex systems of our interest are *ecosystem-like*. Good examples are reaction networks and gene regulatory networks in living organisms in evolutionary time scale, brain and immune system in developmental timescale, engineering systems with decentralized control scheme, ecosystems of companies or products, and

T. Shimada (✉)
Department of Applied Physics, Graduate School of Engineering, The University of Tokyo, 7-3-1 Hongo, Bunkyo-ku, Tokyo 113-8656, Japan

JST CREST, 4-1-8 Honcho, Kawaguchi, Saitama 332-0012, Japan
e-mail: shimada@ap.t.u-tokyo.ac.jp

Y. Murase
JST CREST, 4-1-8 Honcho, Kawaguchi, Saitama 332-0012, Japan

RIKEN AICS, 7-1-26, Minatojima-minami-machi, Chuo-ku, Kobe, Hyogo 650-0047, Japan
e-mail: yohsuke.murase@riken.jp

N. Ito
Department of Applied Physics, Graduate School of Engineering, The University of Tokyo, 7-3-1 Hongo, Bunkyo-ku, Tokyo 113-8656, Japan

JST CREST, 4-1-8 Honcho, Kawaguchi, Saitama 332-0012, Japan

RIKEN AICS, Minatojima-minami-machi, Chuo-ku, Kobe, Hyogo 650-0047, Japan
e-mail: ito@ap.t.u-tokyo.ac.jp

H. Takayasu et al. (eds.), *Proceedings of the International Conference on Social Modeling and Simulation, plus Econophysics Colloquium 2014*, Springer Proceedings in Complexity, DOI 10.1007/978-3-319-20591-5_9

social communities. In those ecosystem-like systems, there is no top-down or centralized mechanism for the system's growth and maintenance. And their complexity emerges as a result of successive introductions of new elements. In the following, we focus on the universal aspects of robustness of such ecosystem-like systems.

The robustness (or stability, fragility, resilience, etc.) of complex systems itself is indeed a classical problem [1]. Essential theoretical findings those have been found on this issue include the general instability of large and densely interacting systems [2], the self-organized criticality [3], and the relation between the robustness and the network structure of the systems [4, 5]. However, the key and universal feature of the real complex systems, openness, has not been well considered. Meanwhile, theoretical studies on ecosystems using various different models have indicated that they share universal behaviors independent of the detail of the dynamics [6–10]. Therefore it is natural to ask how can such ecosystem-like system grow to more complex structure by adding new elements to it, using a simpler model. In the following, we first introduce a minimal model for this problem and show that it yields a novel type of transitions, together with its underlying mechanism [11]. Then we show an example of direct relation between the minimal model and the more detailed nonlinear dynamical models, which corroborates the relevance of the newly found mechanism to the real phenomena.

9.2 A Universal Relation Between Robustness and Connection

9.2.1 A Minimal Model of Evolving Open Systems

We here introduce a minimal model of evolving open systems [11]. In this model, the entire system is structured as a collection of nodes connected by directed and weighted links (Fig. 9.1). The nodes may represent various kinds of *species* (e.g. chemical species, different genes and proteins, neurons, animal species, companies, products, individuals, etc.). In the following, we simply call them species. Also the links may represent diverse kinds of interactions (or inputs, signal, influences, effects, etc.) among them. The directed link from species j to species i with its link weight denotes the influence of species j on species i. Each species has only one property, *fitness*, which is simply determined by the sum of its incoming interaction weights from other species in the system. Only the rule intrinsic to the system is that each species can survive as long as its fitness is greater than zero, and otherwise it goes extinct. If the minimum fitness in the system is non-positive, we delete that species (therefore totally isolated species cannot survive). Because this extinction will modify the fitness of the other species, we re-calculate the fitness and re-identify the least-fit species. We continue this deletion procedure until the minimum fitness becomes positive, meaning that the system is stable. Once the system gets to a stable state, nothing will happen in terms of this intrinsic fast process. Therefore

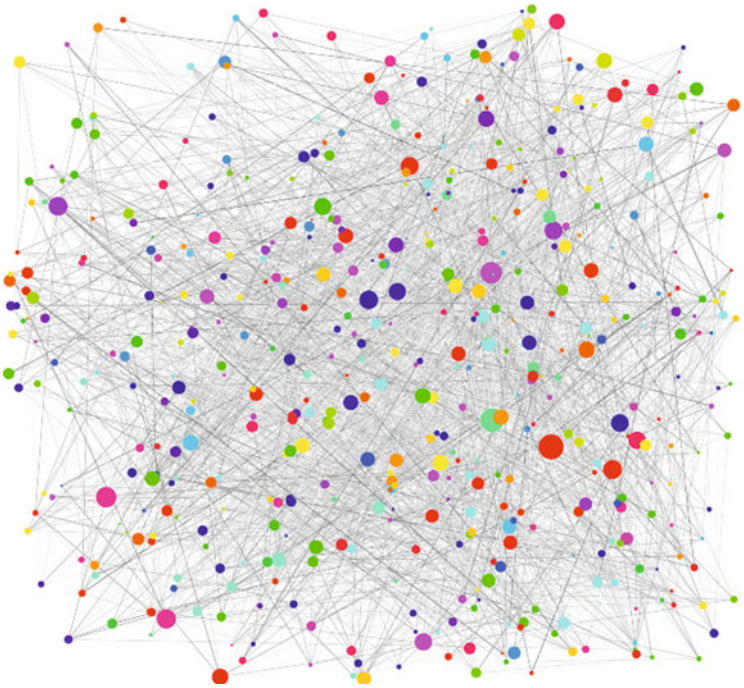

Fig. 9.1 A snapshot of ecosystem-like system obtained from the minimal model described in the Sect. 9.2.1. *Nodes* and *links* represent the general gspeciesh and ginteractionsh respectively. While the diameter of each cnode depicts the current fitness, its color is just for visibility

we proceed the time by the order of magnitude of longer unit i.e. the evolutionary time scale (in some other systems, it corresponds to the developmental time scale and so on). At each evolutionary time step t, a new species is added into the system. We establish interactions from and to the newly added species. The interacting species are chosen randomly from the resident species with equal probability, and the directions of the interactions are also determined randomly. The link weights are assigned randomly from a zero-mean distribution (for example, the standard normal distribution). Then, we re-calculate the fitness of each species to find whether the system can accommodate the new species or some species should become extinct. We repeat this addition-and-deletion steps. Note that the behavior of the system after a sufficiently large number of time steps does not depend on the initial condition. Therefore, this model has only one relevant parameter: m, the number of interactions per species. For clarity, we show below the pseudo-code of this model.

```
// Pseudo-code of the minimal model
Create an initial state with N species
Check the extinctions as described below

FOR t = 0 to t_max
   Add a new species
```

```
    FOR each of m new links
       Choose an interacting species randomly
        from resident species
       Choose the direction of the link randomly
        with equal probability 0.5 for each direction
       Assign the link weight a_ij randomly
        from a 0 mean distribution
    ENDFOR

    Flag_ext = true
    WHILE Flag_ext
       FOR each species
          f_i = 0
          FOREACH incoming links j
             f_i += a_ij
          ENDFOR
       ENDFOR
       Find the species k which has minimum fitness f_min
       IF f_min <= 0
          Delete species k
          Delete the links from/to it
       ELSE
          Flag_ext = false
       ENDIF
    ENDWHILE
    Observe the current stable community
ENDFOR
```

9.2.2 Transition in Growth Behavior

In the present model, the essential features of the ecosystem-like systems, the introduction of a new species and the interaction-dependent survival condition for each species, are took into account. And because the both processes are introduced in neutral way, i.e. giving no apparent advantage to grow or collapse. Therefore whether the system can grow under such process will purely illuminate the relation between the system's complexity and robustness. Simulation results indeed give a fascinating answer: both of the growth and collapse can happen, depending on the only one model parameter m. The system can grow to infinitely large size if the number of interactions per species is in a moderate range (for the case of taking the standard distribution for link weights, the range is $5 \leq m \leq 18$), and, if not, it stays in a finite size (Fig. 9.2).

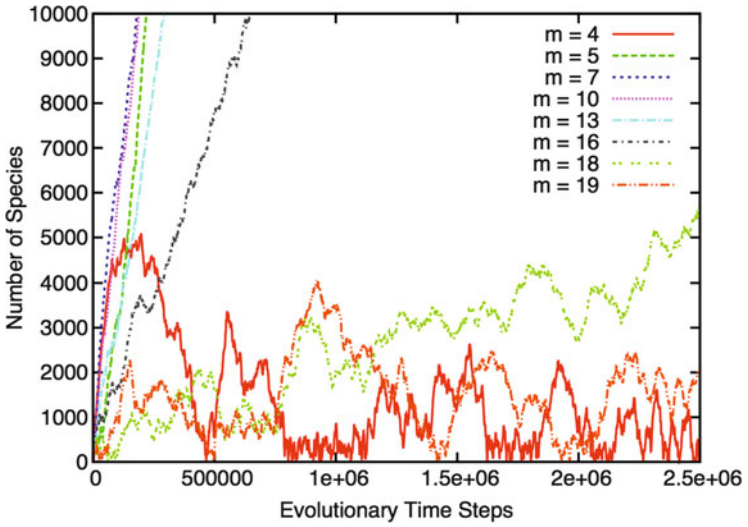

Fig. 9.2 Temporal evolutions of the number of species. The number of species diverges if $5 \leq m \leq 18$. For more precise and reliable determination of the transition point in this behavior needs systematic and longer simulations (see [11])

9.2.3 A Mean-Field Analysis and the Transition Mechanism

The first transition at between $m = 4$ and 5 turns out to be related to a kind of percolation threshold: the emergent system with too sparse interactions can have only tree-and-cycle-like network, and therefore it is too fragile to continue growing. But then why we have another transition in the denser interaction regime? This latter transition is non-trivial and novel, and therefore we mainly focus on this in this paper.

To consider the mechanism of the transition, we first investigate the topology of the emerging network. We can confirm that there is no strong structure in the emerging networks (Fig. 9.1). In other words, the structure of the emerging system remains almost random network with average degree $\sim m$. From this observation, a theoretical analysis based on a mean-field picture has been performed [11, 12]. In this theory, we only treat the distribution function of the fitness of the species in the entire community. Because the fitness distribution function (FDF) is dependent on the parameter m, we write the FDF of fitness x as $F(m, x)$. FDF of the newly introduced species, which has $m/2$ incoming links on average, is easily calculated as the positive half of the normal distribution with variance $\frac{m}{2}$:

$$F_0(m,x) = \begin{cases} 0 & (x \leq 0) \\ 2G(\sigma_m, x) & ensuremath(x \geq 0) \end{cases}, \quad \sigma_m = \sqrt{\frac{m}{2}}. \tag{9.1}$$

Where $G(\sigma, x)$ denotes the normal distribution with its deviation σ. After settling to the system, the species will experience either obtaining a new link from a newly introduced species or loosing a link during the extinction of interacting species. Those processes change the fitness of the species, and hence the distribution function. This change in FDF is found to be the one step of random walk with negative drift whose strength is proportional to $1/m$. Therefore, writing this process by an operator $\hat{\mathscr{D}}$, the (not normalized) FDF of species those have been experienced a loss or addition of one incoming link can be calculated from F_0 as,

$$F_1(m,x) = \hat{\mathscr{E}}\hat{\mathscr{D}}F_0(m,x), \tag{9.2}$$

where $\hat{\mathscr{E}}$ is the extinction operator which cut the negative part of any function:

$$\hat{\mathscr{E}}h(x) = \begin{cases} 0 & (x \le 0) \\ h(x) & (x \ge 0) \end{cases}. \tag{9.3}$$

Note that the operators $\hat{\mathscr{D}}$ and $\hat{\mathscr{E}}$ are non-commutative. In the following we call the suffix g of F_g, the number of incoming link addition/deletion events that species has experienced, as *generation*. As we have seen, calculation of the FDF of generation g needs the FDF of younger generation, $g-1$:

$$F_g(m,x) = \hat{\mathscr{E}}\hat{\mathscr{D}}F_{g-1}(m,x), \tag{9.4}$$

Only after performing the iterative calculation, we obtain the probability distribution function of the fitness of the entire system,

$$F(m,x) = \frac{\displaystyle\sum_{g=0}^{\infty} F_g(m,x)}{\displaystyle\sum_{g=0}^{\infty} n_g(m)} \quad \left(n_g(m) = \int_0^\infty F_g(m,x)dx \right), \tag{9.5}$$

which contains all the information we need under the mean-field approximation. The most important outcome from the FDF is the average probability of entire resident species going extinct during one link addition/deletion event E, which is calculated as

$$E(m) = 1 - \int_0^\infty \hat{\mathscr{E}}\hat{\mathscr{D}}F(m,x)\,dx = \frac{\displaystyle\int_0^\infty F_0(m,x)\,dx}{\displaystyle\sum_{g=0}^{\infty} n_g(m)} = \frac{1}{\displaystyle\sum_{g=0}^{\infty} n_g(m)}. \tag{9.6}$$

From this calculation, we find that E is a decreasing function of m. Therefore the *robustness of each species* against the disturbance increases with m.

What should be emphasized, however, is that the robustness of each species does not directly determine the *robustness of the entire system*. Let us see this using an infinitely large graph in which all the nodes have m links. The average number of species that go extinct directly because of an inclusion of the new species is simply calculated as $mE/2$. Because those extinctions may also trigger sequential extinctions, the expectation value of the total number of extinctions per inclusion of one species N_E is simply calculated from an infinite geometric series as

$$N_E = \sum_{n=1}^{\infty} \left(\frac{mE}{2}\right)^n = \frac{mE}{2 - mE}. \tag{9.7}$$

Therefore the *robustness of the entire system* is a function of mE, not the bare E. And because $N_E = 1$ means that the average number of extinctions balances with the number of inclusions in the long time average, that corresponds to the transition point of the growth behavior. In other words, the following self-consistent condition should be satisfied for the critical number of interactions per species: $m_* E(m_*) = 1$.

Let us now focus on the relevant parameter in the argument above, mE. We find that the decrease of E is slower than $1/m$ (roughly $\sim 1/\sqrt{m}$). Therefore mE is a sub-linearly increasing function of m, and it crosses the critical value 1 around $m_* = 13$. This means that the mean-filed treatment can explain the transition in the growth behavior of the system. In addition, this theory give us the simple understanding of the transition mechanism. It originates from the balance of the two effects: although having more interactions makes each species robust against the disturbances (addition and extinction of the species relating to that species), it also increases the impact of the loss of a species. In consistent with this success in explaining the transition by the mean-field analysis, we can find essentially same phase diagram in slightly modified models, such as the model with giving a randomly distributed degrees for the newly added species, the one with different distribution functions for the link weights, and so on [11].

In the classical diversity-stability relation based on the linear stability of dynamical systems, an intrinsic stability is assumed for each element to ensure the stability of each element when that has no interactions. For the system to remain stable, each element may have essentially only one interaction that is not weak comparing to the given intrinsic stability [2]. In the present mechanism, we do not assume any kind of intrinsic stability to the elements: an element with no interaction immediately goes extinct. Even so, the system with 10 or more interactions per element can grow. In this sense, the condition we have identified is very realistic. Indeed in the real systems, it is quite often to find moderately sparse networks: the average degree is in the order of 10, not order of 1, and that seems not dependent on the system size. This novel relation between the connection in the system and its robustness might be a origin of this.

9.3 The Relation with More Complex Dynamical Models

We have reviewed a novel relation between the system's robustness and the connections in it using a very simple model. In our simple model, the extinction condition $f_i \leq 0$ represents the system's intrinsic dynamics. The simplicity of the model is good in terms of universality, and hence especially good for applying to social and economic systems because it is very hard to obtain precise equation of motion or evolution rule of those. And the fact that we can find a good agreement between the model and real systems in their statistics encourages us to put more emphasis on universality. A good example is lifetime distribution function of the species [13, 14].

However, for each certain problem, we generally treat more complex models. Therefore it would be nice if we can argue more directly about the connection between our simple model and complex models. In the following, we will consider a certain class of population dynamics models and show that the necessary condition to have extinctions in it reduces to the extinction rule in the simple model.

9.3.1 The Extinction Condition in Population Dynamics Models

In many dynamical models, each element has more properties in addition to its mere existence and the interactions depend on those properties. One of the most popular class is population dynamics models, in which each element has its property, population x_i. The general form of the dynamical equation of motion of population dynamics models can be written as,

$$\dot{x}_i = f_i(x_1, x_2, \cdots, x_N), \tag{9.8}$$

where the dynamical variable $\{x_i\}$ denote the population of element i. To know which species will go extinct is generally a difficult problem, because one needs to have the trajectory. This is one of the reason why so many studies substitute the stability of the system for its linear stability, which is, strictly speaking, neither enough condition nor necessary condition to really determine the fate of the species. The necessary condition to have an extinction of certain species is relatively easier, because it is at least describable simply: the necessary condition to go extinct is to satisfy

$$\lim_{x_i \to 0} \dot{x}_i = f_i(x_1, \cdots, x_{i-1}, 0, x_{i+1}, \cdots, x_N) < 0 \tag{9.9}$$

at somewhere in the $x_i = 0$ surface. Such condition is again generally difficult to access and also different from the linear stability condition.

9.3.2 Ratio-Dependent Interactions

The interaction term in the population dynamics with the form of $f_{ij}\left(\frac{x_i}{x_j}\right)x_j$, in which the predation rate per predator j, $f_{ij}(\xi)$, is an arbitrary function of the ratio of the prey to the predator x_i/x_j, is called ratio-dependent form in theoretical ecology and regarded as a realistic model of the predation interaction [15]. A typical simple example of the form of $f(\xi)$ is

$$f(\xi) = \frac{B\xi}{A+\xi}, \tag{9.10}$$

where A and B are constants. If we neglect many-body effects such as the competition among the predators those attack the same prey, the predator's choice on multiple preys, and so on for simplicity (otherwise the dynamical equations may become implicit), the population dynamics of such systems can be written as

$$\dot{x}_i = \sum_j f_{ij}\left(\frac{x_i}{x_j}\right)x_j + \sum_k f_{ki}\left(\frac{x_k}{x_i}\right)x_i, \tag{9.11}$$

where the summations run for the predators and the preys of species i, respectively.

9.3.3 The Necessary Condition to Have an Extinction Under "natural" Ratio-Dependent Interactions

Let us next limit the case by postulating the following relatively natural features to the ratio-dependent predation rate. That is, $f(\xi)$ must go to 0 as the population of the prey goes to 0 and that must saturate at a certain value when the population of the prey is abundant, i.e.

$$\lim_{\xi\to 0} f_{ij}(\xi) = 0 \ \cap \ \lim_{\xi\to\infty} f_{ij}(\xi) = b_{ij}, \tag{9.12}$$

where b_{ij} represents the maximum predation rate on that interaction. The example we have seen in Eq. (9.10) satisfies these both features. And if we suppose it does not have any singularity around 0, we can obtain its Maclaurin series as,

$$f_{ij}\left(\frac{x_i}{x_j}\right)x_j = \left[\sum_{n=1}^{\infty} c_n^{ij}\left(\frac{x_i}{x_j}\right)^n\right]x_j. \tag{9.13}$$

Where

$$c_n^{ij} = \frac{1}{n!} \cdot \left. \frac{d^n f_{ij}(\xi)}{d\xi^n} \right|_{\xi \to 0} \tag{9.14}$$

is the coefficient of Taylor series expansion at 0. This means that the necessary condition for the extinction [Eq. (9.9)] of species i in this model is indeed not dependent on the populations of the surrounding species:

$$\begin{aligned} \lim_{x_i \to 0} \dot{x}_i &= \lim_{x_i \to 0} \left[\sum_j \left\{ \sum_{n=1}^{\infty} c_n^{ij} \left(\frac{x_i}{x_j} \right)^n x_j \right\} + \sum_k f_{ki} \left(\frac{x_k}{x_i} \right) x_i \right] \\ &= \left[\sum_j c_1^{ij} + \sum_k b_{ki} \right] x_i < 0. \end{aligned} \tag{9.15}$$

And this condition, $\sum_j c_1^{ij} + \sum_k b_{ki} < 0$, that says summation of the population-independent coefficients assigned to the interacting links should be negative, is exactly in the same class with the minimal model we introduced in Sect. 9.2.1.

9.4 Conclusion

We have reviewed the simple and universal mechanism of determining the robustness, and therefore its ability to grow, of ecosystem-like systems by introducing a simple model. It has been also shown that the necessary condition for extinctions in a certain type of dynamical models essentially result in the same condition with that of the simple model. This supports our future approach to verify the relevance of the newly found mechanism to the real phenomena.

Acknowledgements This work was partially supported by JSPS Grant-in-Aid for Scientific Research (C) Grant Number 15K05202.

References

1. MacAuthor R (1955) Fluctuations of animal populations, and a measure of community stability. Ecology 36:533–535
2. Gardner MR, Ashby WR (1970) Connectance of large dynamic (cybernetic) systems: critical values for stability. Nature 228:784
3. Bak P, Sneppen K (1993) Punctuated equilibrium and criticality in a simple model of evolution. Phys Rev Lett 71:4083–4086
4. Albert RJ, Jeong H, Barabási A-L (2000) Error and attack tolerance of complex networks. Nature 406:378–382
5. Herrmann HJ, Schneider CM, Moreira AA, Andrade JS, Havlin S (2011) Onion-like network topology enhances robustness against malicious attacks. J Stat Mech 2011:P01027
6. Taylor PJ (1988) Consistent scaling and parameter choice for linear and generalized lotka-volterra models used in community ecology. J Theor Biol 135:543–568
7. Caldarelli G, Higgs PG, McKane AJ (1988) Modelling coevolution in multispecies communities. J Theor Biol 193:345–358
8. Shimada T, Yukawa S, Ito N (2002) Self-organization in an ecosystem. Artif Life Robotics 6:78–81
9. Perotti JI, Billoni OV, Tamarit FA, Chialvo DR, Canna SA (2009) Emergent self-organized complex network topology out of stability constraints. Phys Rev Lett 103:108701
10. Murase Y, Shimada T, Ito N, Rikvold PA (2010) Random walk in genome space: a key ingredient of intermittent dynamics of community assembly J Theor Biol 264:663–672
11. Shimada T (2014) A universal transition in the robustness of evolving open systems. Sci Rep 4:4082
12. Shimada T (2015) In: Mathematical approaches to biological systems. Ohira T, Uzawa T (eds) Springer, Japan, pp 95–117
13. Shimada T, Yukawa S, Ito N (2003) Life-span of families in fossil data forms q-exponential distribution Int J Mod Phys C 14:1267–1271
14. Murase Y, Shimada T, Ito N (2010) A simple model for skewed species-lifetime distributions New J Phys 12:063021
15. Drossel B, Higgs PG, Mckane AJ (2001) The influence of predator prey population dynamics on the long-term evolution of food web structure. J Theor Biol 208:91–107

Chapter 10
Simulation of Gross Domestic Product in International Trade Networks: Linear Gravity Transportation Model

Tsuyoshi Deguchi, Hideki Takayasu, and Misako Takayasu

Abstract In this study, we introduce a model to simulate gross domestic product (GDP) for international trade network data. By applying a linear gravity transportation model, we confirm that estimated values approximately agree with the real values of GDP by tuning the model parameters. An exception is the estimated GDP of China that is about two times bigger than the real value. This discrepancy might imply that China's GDP is not saturated and it is on the way of growing.

10.1 Introduction

Today, China is becoming increasingly influential in not only the international community but also international politics and military forces. However, its presence is most notable in the international economy. In particular, with China's growing gross domestic product (GDP), the country has the potential to become the biggest economy in the near future. GDP is the most specific and popular measure in the economic statistics literature, although many have doubted China's GDP statistics [1, 2].

T. Deguchi (✉) • M. Takayasu
Department of Computational Intelligence and Systems Science, Interdisciplinary Graduate School of Science and Engineering, Tokyo Institute of Technology, 4259 Nagatsuta-cho, Midori-ku, Yokohama 226-8502, Japan
e-mail: deguchi.t.ad@m.titech.ac.jp; takayasu@dis.titech.ac.jp

H. Takayasu
Sony Computer Science Laboratories, 3-14-13 Higashigotanda, Shinagawa-ku, Tokyo 141-0022, Japan

Graduate School for Advanced Mathematical Sciences, Meiji University, 4-21-1 Nakano, Nakano-ku, Tokyo 164-8525, Japan

Department of Computational Intelligence and Systems Science, Interdisciplinary Graduate School of Science and Engineering, Tokyo Institute of Technology, 4259 Nagatsuta-cho, Midori-ku, Yokohama 226-8502, Japan
e-mail: takayasu@csl.sony.co.jp

H. Takayasu et al. (eds.), *Proceedings of the International Conference on Social Modeling and Simulation, plus Econophysics Colloquium 2014*, Springer Proceedings in Complexity, DOI 10.1007/978-3-319-20591-5_10

In this paper, we estimate and simulate countries' GDP and ranks using the linear gravity transportation model (LGTM). The gravity transportation model (GTM) is known to be effective in examining a company's transaction networks [3, 4]. The LGTM is a linearized form of the GTM and is a type of degree distribution model [5, 6].

10.2 Preceding Study

International trade networks (ITNs) are predominantly used in surveying network structures and known to follow the so-called "gravity relation" [7]. They were first examined in 2003 by Serrano and Boguñá, who presented the fundamental characteristics of ITNs for different countries [8]. Recently, physicists and network researchers have explored the structure on the basis of diverse factors, such as time series robustness, community structures, and inter-layer dependency [9–12]. Some researchers have attempted to extend ITN research to that on economic growth [13–16]. These studies contribute some interesting findings from the viewpoint of complex networks. For instance, Garlaschelli et al. found that GDP is a hidden factor that influences networks [17]. Although this fact is common knowledge in international economics, their model remains an impressive contribution to network study. Several other studies have been conducted on gravity relations [18–20].

10.3 Dataset

We adopt data from the Direction of Trades Statistics (DOTS) compiled by the International Monetary Fund (IMF) [21]. This dataset includes annual and monthly data of trades (US dollar) for countries. We use a total of 214 countries (regions) as nodes and their respective trade amounts as weighted links. The weighted links suggest bilateral trade relationships, that is, exports and imports, between countries or regions on a monthly and yearly basis, which are measured in million US dollar. DOTS also include the base data for both exports and imports. In general, the amount of export from country A to country B should be same as the amount of import to country B from country A. However, these numbers differ between the import base and export base datasets. In this case, we use the export base year dataset.

We also use GDP data from the Economic Outlook Dataset, also produced by IMF. We use this data with enough credit. However, this dataset includes only 189 countries. Thus, we arrange these datasets and aggregate ITN and GDP data.

After data processing, we used 2010 ITN and GDP data for 160 countries.

10.4 Simulation Setup

10.4.1 GDP Transaction Flow Relationship

First, we define ITN as an adjacency matrix, W, whose component, w_{ij}, represents the annual amount of transaction flow (imports) from country i to country j, measured in million US dollars. Then, we define $w_{ii} = 0$. We also introduce the binary network matrix, A, whose component $a_{ij} = 1$ when $w_{ij} > 0$ and $a_{ij} = 0$ when $w_{ij} = 0$.

The following relationship between GDP and transaction flows is often assumed in the international trade literature[7].

$$w_{ij} = G\frac{Y_i^{\alpha} Y_j^{\beta}}{R_{ij}^{\gamma}}. \tag{10.1}$$

Here, Y_i is the GDP of node i and R_{ij} is the distance between nodes i and j. The power exponent α, β, and γ are parameters. We neglect the distance R_{ij} and estimate the exponents α and β using data shown in Fig. 10.1.

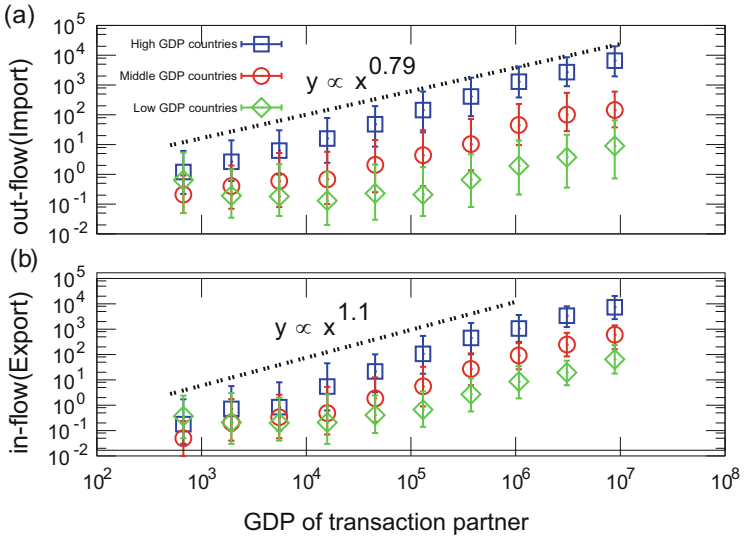

Fig. 10.1 GDP Transaction flow (import and export) relationship in a log-log plot. (**a**) Import (**b**) Export for high GDP countries (top one-third of high GDP countries), middle GDP countries (other countries not classified as high and low GDP countries), and low GDP countries (bottom one-third of high GDP countries). In this case, high, middle, and low GDP relates to the total GDP. Here, bins are defined at regular intervals in log-scale, the first and third quantiles are plotted as error bars with the median value at the center of symbols, *squares* and *circles*

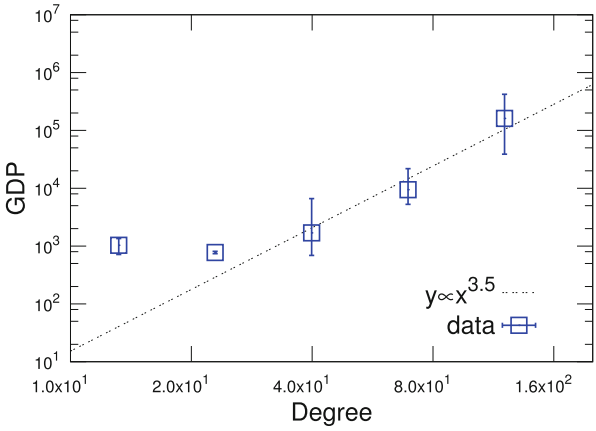

Fig. 10.2 GDP–degree relationship in a log-log plot. The first and third quantiles are plotted as error bars with the median value at the *center of squares*

$$w_{ij} \propto Y_i^{\alpha} Y_j^{\beta}. \tag{10.2}$$

Using parameter fitting, we estimate the values of α and β as $(\alpha, \beta) = (0.79, 1.1)$.

10.4.2 GDP–Degree Relationship

The number of trade parameters is higher for high GDP countries. We confirm the following power law relationship between the degrees and GDPs (Fig. 10.2). Here, we define the in-degree as $k_M = \sum_i a_{iM}$.

$$Y_M \propto {k_M}^{\zeta}. \tag{10.3}$$

Using the data, we estimate $\zeta = 3.5$ (Fig. 10.2).

10.4.3 Linear Gravity Transportation Model

From Figs. 10.1 and 10.2, we know that the amount of trades, degrees and GDPs have positive relations. Thus, we model these relations as a transportation model. In this model, we think the number of degrees directly affects the amount of trade flow, where in-degree is defined as $k_j = \sum_i a_{ij}$. And we calculate the GDPs as a result of the distributions of trades flows using gravity relation. We call this model as a LGTM, which is conceptually depicted in Fig. 10.3.

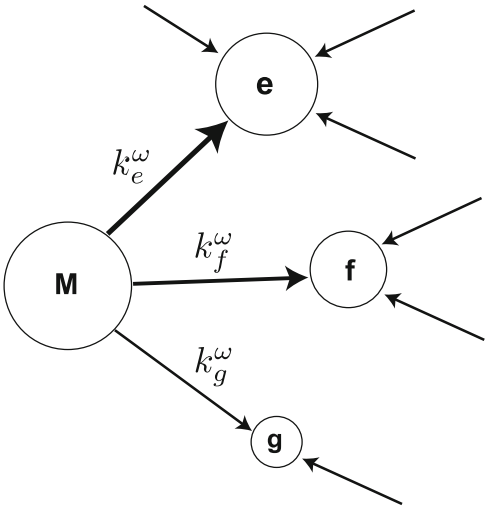

Fig. 10.3 Conceptual figure of weights of out-flow from a node in LGTM. In this case, the amounts proportional to GDPs are transported and distributed to neighbor nodes that are proportional to the ω-th power of other nodes' in-degrees

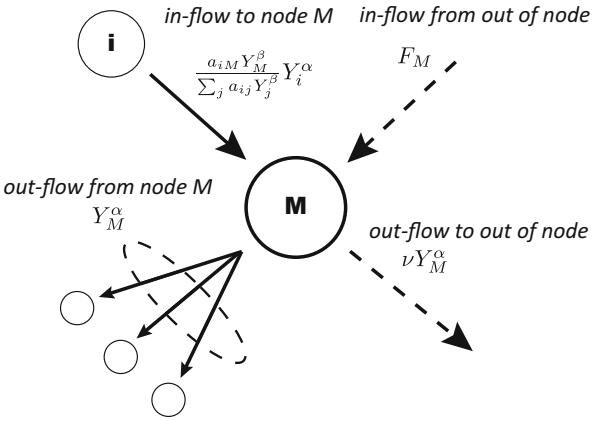

Fig. 10.4 Conceptual figure of all in-flows and out-flows for a node M in LGTM. The *black arrows* denote inflow-outflow relationships among nodes and the *dotted ones* show flow relationships outside of the network

LGTM is based on four types of flows. In the case of node M, inflow in an inter-node relationship is defined as $\frac{a_{iM}k_M^\omega}{\sum_j a_{ij}k_j^\omega}Y_i^\alpha$, which is affected by the degrees. Total outflow from node M in the inter-node relationship is Y_M^α. Inflow and outflow outside of the inter-node relationship are F_M and νY_M^α, respectively (Fig. 10.4). In the equilibrium, the aggregation of all flows is assumed to be zero.

$$\sum_i \frac{a_{iM}k_M^\omega}{\sum_j a_{ij}k_j^\omega}Y_i^\alpha - (1+\nu)Y_M^\alpha + F_M = 0. \tag{10.4}$$

10.5 Simulation Results

Using LGTM, we estimate the GDPs for the given ITN data. First, we must acquire LGTM's parameters $(\alpha, \omega, \nu, F_M)$ from the real data's parameter fitting. Then, we estimate α and ω by minimizing the following function:

$$F(\alpha, \omega) = \sum_i \sum_M \left\{ log \left(\frac{w_{iM}}{\frac{a_{iM} k_M^{\omega}}{\sum_j a_{ij} k_j^{\omega}} Y_i^{\alpha}} \right) \right\}^2 . \tag{10.5}$$

Next, we derive ν from the inflow-outflow relationship in Eq. (10.6) as a transformation of equilibrium (10.4). Here, Y_M^{α} equals outflow (imports) and $\sum_i \frac{a_{iM} k_M^{\omega}}{\sum_j a_{ij} k_j^{\omega}} Y_i^{\alpha}$ equals inflow (exports). Thus, we get $\frac{1}{(1+\nu)}$ as the regression coefficient.

$$Y_M^{\alpha} = \frac{1}{(1+\nu)} \sum_i \frac{a_{iM} k_M^{\omega}}{\sum_j a_{ij} k_j^{\omega}} Y_i^{\alpha} + \frac{F_M}{(1+\nu)}. \tag{10.6}$$

Therefore, we get F_M from the equilibrium in Eq. (10.7).

$$F_M = \frac{\nu \sum_i Y_M^{\alpha}}{N} \tag{10.7}$$

We obtain the values as $(\alpha, \omega, \nu, F_M) = (0.68, 4.5, 0.032, 1.3 \times 10^2)$.

In the case of ITN, there are little differences among top countries' degrees. We introduce the preferentially selected network [6]—a simplified network produced from the original one, in which links with small contributions are removed using the following rule: For all nodes, we select the top n^{th} weight links for both inflow and outflow and cut off all other links. In this simulation, we use the case of preferentially selected network, where $n = 6$.

Under these conditions, we estimate GDP using Eq. (10.6) (Fig. 10.5). We find that the results between the real and simulated GDPs are fairly close. If the real and simulated values are proportionate, the values are assumed to be on the 45 degree line.

Next, we check the top 20 countries for both the simulated and real GDP. The results are listed in Table 10.1. In the real data, China ranks second, whereas in the simulation, it is at the top. China's estimated GDP is about two times bigger than the real GDP. This discrepancy might be caused by slow time evolution that China's GDP is on the way of approaching to the equilibrium value which is determined by the trading network structure. Simulation results are based on the equilibrium and China's GDP would be bigger in near future from the viewpoint of trade.

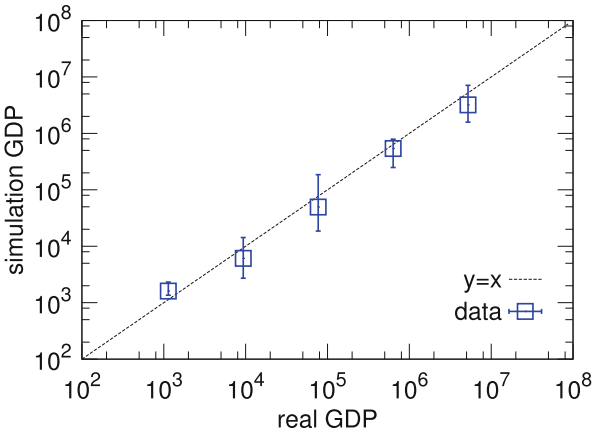

Fig. 10.5 Real and simulated GDPs estimated using Eq. (10.6) and preferentially selected network ($n = 6$). The first and third quantiles are plotted as error bars with the median value at the *center of squares*

Table 10.1 Top 20 countries (real and simulated data)

Country	Real GDP	Simulated GDP	Real rank	Simulated rank
United States	1.5×10^7	8.2×10^6	1	2
China	5.9×10^6	1.2×10^7	2	1
Japan	5.5×10^6	4.7×10^6	3	4
Germany	3.3×10^6	6.7×10^6	4	3
France	2.7×10^6	1.7×10^6	5	6
United Kingdom	2.3×10^6	1.5×10^6	6	9
Brazil	2.1×10^6	1.4×10^6	7	11
Italy	2.1×10^6	1.6×10^6	8	8
India	1.7×10^6	1.2×10^6	9	12
Canada	1.6×10^6	5.9×10^5	10	22
Russia	1.5×10^6	8.8×10^5	11	16
Spain	1.4×10^6	3.9×10^5	12	33
Australia	1.2×10^6	1.1×10^6	13	15
Korea	1.1×10^6	2.4×10^6	14	5
Mexico	1.1×10^6	1.0×10^4	15	95
Netherlands	8.4×10^5	1.7×10^6	16	7
Turkey	7.3×10^5	5.7×10^5	17	24
Indonesia	7.1×10^5	1.1×10^6	18	13
Switzerland	5.5×10^5	6.0×10^5	19	21
Saudi Arabia	5.3×10^5	4.5×10^5	20	30

In this simulation, we use parameters $(\alpha, \omega, \nu, F_M)$ in three significant digits and simulation results are represented in two significant digits

10.6 Conclusion

In this paper, we empirically introduced a linear gravity transportation model of world trade based on the network structure among countries. By tuning the model's parameters, we confirmed that estimated values approximately agree with the real

values of GDP. One apparent exception is China that its estimated GDP value is about two times bigger than the real value. This discrepancy might imply that China's GDP is growing rapidly and the steady state solution of our model for given world trade network structure does not fit well.

Acknowledgements This work was supported by a Grant-in-Aid for Scientific Research (B), Grant Number 26310207 and a Grant-in-Aid for Scientific Research (C), Grant Number 24540395.

References

1. Rabinovitch S, Chinese econ stats: to doubt or not to doubt. (Financial Times, 28 June 2012), http://blogs.ft.com/beyond-brics/2012/06/28/china-stats-to-doubt-or-not-to-doubt. Accessed 30 Jan 2015
2. Rawski T (2001) China Econ Rev 12:347–354
3. Tamura K, Miura W, Takayasu H, Kitajima S, Goto H, Takayasu M (2012) Proceedings of the Asia Pacific symposium on intelligent and evolutionary systems, Kyoto, Japan. (ISBN978-4-99066920-1, 2012)
4. Tamura K, Miura W, Takayasu M, Takayasu H, Kitajima S, Goto H (2012) Int J Mod Phys Conf Ser 16:93–104
5. Watanabe H, Takayasu H, Takayasu M (2012) New J Phys 14:043034
6. Deguchi T, Takayasu H, Takayasu M. In preparation
7. Krugman P, Obstfeld M, Melitz M (2011) International economics: theory and policy, 9th edn. Pearson Education, Boston
8. Serrano M, Boguñá M (2003) Phys Rev E 68:015101
9. Garlaschelli D, Loffredo M (2005) Physica A 355(1):138–144
10. Fagiolo G, Reyes J, Schiavo S (2009) Phys Rev E 79:036115
11. Tzekina I, Danthi K, Rockmore D (2010) Eur Phys J B 63:541–545
12. Barigozzi M, Fagiolo G, Garlaschelli D (2010) Phys Rev E 81:046104
13. Hidalgo C, Klinger B, Barabási A, Hausmann R (2007) Science 317:482–487
14. Hidalgo C, Hausmann R (2009) Proc Natl Acad Sci 106:10570–10575
15. Tacchella A, Cristelli M, Caldarelli G, Gabrielli A, Pietronero L (2012) Sci Rep 2:723
16. Zaccaria A, Cristelli M, Tacchella A, Pietronero L PloS one (2014) 9:e113770
17. Garlaschelli D, Loffredo M (2004) Phys Rev Lett 93:188701
18. Fagiolo G (2010) J Econ Interact Coord 5:1–25
19. Dueñas M, Fagiolo G (2013) J Econ Interact Coord 8:155–178
20. Almog A, Squartini T, Garlaschelli D (2015) New J Phys 17:013009
21. Direction of trade statistics. In: IMF eLibrary data. http://elibrary-data.imf.org. Accessed 30 Jan 2015

Chapter 11
Analysis of Network Robustness for a Japanese Business Relation Network by Percolation Simulation

Hirokazu Kawamoto, Hideki Takayasu, and Misako Takayasu

Abstract This paper describes the application of percolation theory to a Japanese business relation network composed of approximately 3,000,000 links. In this network, we examined the process in which links are randomly removed. At the percolation transition point, we calculate the survival rate for each node as an indicator of its global network connectivity. The basic properties of each node are determined in connection with the values characterising these complex networks, such as the link number and job category. We confirm that this index has strong correlation with degree and shell number, also has significant correlation with sales and number of employee. Finally, we define the network robustness for each prefecture in Japan by using this new indicator.

11.1 Introduction

Percolation theory has been studied in the fields of physics and mathematics. Especially, many interesting properties have been revealed about the percolation transition point at which macroscopic connectivity disappears when removing its elements [1]. Because of the high versatility of this theory, it has been applied to

H. Kawamoto (✉) • M. Takayasu
Department of Computational Intelligence and Systems Science, Interdisciplinary Graduate School of Science and Engineering, Tokyo Institute of Technology, Midori-ku, Yokohama, Japan
e-mail: kawamoto@smp.dis.titech.ac.jp; takayasu@dis.titech.ac.jp

H. Takayasu
Sony Computer Science Laboratories, Shinagawa-ku, Tokyo, Japan

Meiji Institute for Advanced Study of Mathematical Sciences, Meiji University, Nakano-ku, Tokyo, Japan

Department of Computational Intelligence and Systems Science, Interdisciplinary Graduate School of Science and Engineering, Tokyo Institute of Technology, Midori-ku, Yokohama, Japan
e-mail: takayasu@csl.sony.co.jp

H. Takayasu et al. (eds.), *Proceedings of the International Conference on Social Modeling and Simulation, plus Econophysics Colloquium 2014*, Springer Proceedings in Complexity, DOI 10.1007/978-3-319-20591-5_11

a wide range of real world problems, such as electrical conduction [2] and Internet traffic congestion [3].

Since the BA model was proposed [4], percolation theory has been applied to complex networks with an inhomogeneous structure in connection with the concept of small-world [5]. Studying the percolation process in such complex networks plays an important role from the viewpoint of the fragility of a given system. It is well known that scale-free networks lose connectivity at low density if nodes are removed randomly and at high density if nodes are removed in descending order of the degree [6]. Because these studies can be viewed as a kind of stress test, percolation theory is also important for application study.

In the next section, we explain a dataset composed of about 600,000 Japanese firms and describe its basic properties as a complex network. We present the basic results of our percolation simulation in Sect. 11.3. The statistical properties of the survival rate and the theoretical analysis are provided in Sect. 11.4. In Sect. 11.5, we discuss the network robustness of the prefecture in Japan. Finally, we conclude this study and mention our plans for future work in Sect. 11.6.

11.2 Business Relation Network

The dataset we used in this study was provided by TEIKOKU DATABANK, Ltd., a Japanese credit research company. It included information about the direction of money flow, sales and employees of each firm in operation in 2011. From the point of view of a network study, the dataset provided a complex network consisting of 612,133 nodes and 3,841,496 links. As we were interested in the percolation properties of this network, we ignored the direction of the links and severed so-called dangling bonds, i.e. the bonds that could be removed from the network by the removal of a single link. We then extracted the largest strongly connected component (LSCC) from the raw network [7], and ignored the direction of each of the links for simplicity. As a result of this process, our network was composed of 327,721 nodes and 2,960,370 links. This operation enabled us to reduce the amount of numerical calculation in the following analysis.

Next, we present the basic properties of this network. The link number, namely, degree k, is distributed across a wide range, and this distribution is approximated by a power law for a large degree.

$$F(\geq k) \propto k^{-\alpha} \tag{11.1}$$

The cumulative exponent α is roughly estimated to be 1.5. Hence, the business relation network is a typical scale-free network [8]. In addition, it also has the small-world property [9].

In this network, we introduce k-shell decomposition, which is a general method intended to reveal the layer structure in a complex network [10]. Application of this method enabled this network to be decomposed into 25 layers, which are also called shells. A shell number is defined for each node, and the number of nodes with the shell number 7 is most numerous [11].

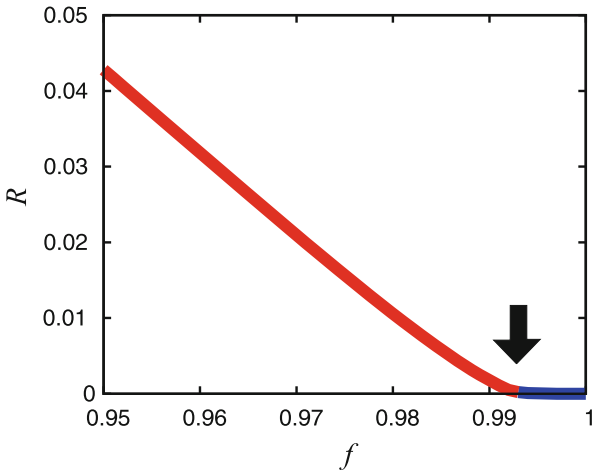

Fig. 11.1 Largest cluster size R normalised by all links in the range of f between 0.95 and 1.00. The arrow indicates the percolation transition point. The average was taken over 100 trials

11.3 Percolation Simulation

A detailed observation of the changes in the network topology became possible when links were randomly removed from the network one by one especially around the percolation transition point. In this case, we did not apply node removal as this could be viewed as a kind of correlated link removal. We calculated the largest cluster size R as an order parameter, which was defined as the ratio of the number of links in the cluster to all the initial links. Here, the control parameter f is the ratio of the number of removed links to all links. As shown in Fig. 11.1, the order parameter R is sufficiently small for f larger than f_c, which is referred to as the percolation transition point. We estimated the value of f_c as 0.994. Its value is approximately 1, but not exactly 1, and this result is consistent with the findings of previous research in which percolation simulation was applied to a complex network [12]. The properties around this point are discussed in detail from the viewpoint of statistical physics including the finite-size effect [11].

11.4 Survival Rate

11.4.1 Basic Properties of Survival Rate

In this section, we introduce the survival rate for each node and provide its basic properties. At the transition point ($f_c = 0.994$), the survival rate is defined as the ratio of the number of trials, in which the node belongs to the largest cluster, to the total number of trials. In this study, 100,000 trials were performed to estimate the value of the survival rate for each node. This parameter is widely distributed, and its large-scale behaviour approximates a power law [11]. It should be noted that this

Table 11.1 Spearman's rank correlation coefficient between the survival rate and principal parameters (degree, shell number, sales, and number of employees)

	Spearman's rank correlation coefficient
Degree	0.729
Shell number	0.765
Sales	0.378
The number of employee	0.356

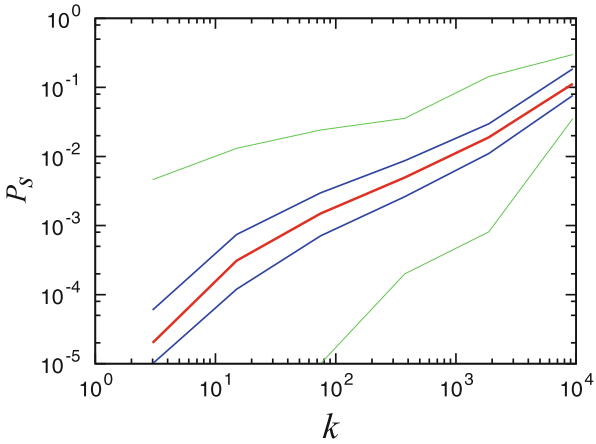

Fig. 11.2 Degree k vs the survival rate P_s in a log-log scale. Minimum, 1st quartile, median, 3rd quartile and maximum are plotted for log bin. In cases where the representative value was 0, we replaced the observation limit, 1.0×10^{-5}

index is able to characterise the global connectivity of each node in the network as we explain in Sect. 11.4.3.

Next, we discuss the correlation between the survival rate and important parameters characterising firms, such as degree, shell number, sales and the number of employees. Spearman's rank correlation coefficient was chosen for this purpose, because Pearson's correlation coefficient is susceptible to outliers. As shown in Table 11.1, there is a positive correlation between the survival rate and all the parameters, and this is especially strong for values characterising the network, such as the degree and shell number.

The correlation between degree k and the survival rate P_s was investigated in more detail. The variation of the survival rate P_s was clarified by plotting its distribution for degree k as shown in Fig. 11.2. We found that the survival rate P_s varies even in the same range of degree k. Therefore, the survival rate P_s is not completely determined by information relating to the local connectivity, such as degree k; the degree k can explain this value roughly. This fact suggests that the survival rate P_s is determined by the critical cluster, which includes the information of the whole network topology. In this sense, this robust index includes information about the global connectivity, such as the shell number, as opposed to local connectivity such as the link number.

Fig. 11.3 Nodes with small survival rate (*red circles*) and its linking nodes (*orange dots*) plotted for Hokkaido Island in Japan

11.4.2 Practical Meaning of P_s

It is important to note that the nodes with the same survival rate P_s were confirmed to have widely distributed link numbers as shown in Fig. 11.2. We subsequently investigated the features of the nodes with a high survival rate for small link numbers and those with a low survival rate for large link numbers. First, we specified a range of degree k from 1 to 10 as a set of small link numbers within a certain range of the survival rate ($5.0 \times 10^{-4} \leq P_s \leq 5.0 \times 10^{-3}$), which includes approximately 20,000 nodes. When we investigated the industry these nodes represent, it was revealed that the nodes categorised as belonging to the construction industry captured 27 % of the share, whereas the share was 21 % of the network in its initial state. This result means that nodes belonging to the construction category have a higher survival rate than nodes in other categories.

Next, we focused on nodes with a large number of links within the same range of survival rate ($5.0 \times 10^{-4} \leq P_s \leq 5.0 \times 10^{-3}$). These nodes are characterised by a low survival rate and are fragile in spite of their many links. As an example, we paid attention to the node with large k and relatively small P_s, $(k, P_s) = (448, 3.3 \times 10^{-3})$. As shown in Fig. 11.3, most of its linking nodes are located on the same island, Hokkaido, and there are only 13 links (about 3 %) connecting to firms outside this island. There are not many links connecting to nodes located outside of this island. This result suggests that this type of node bundles firms in a local region.

11.4.3 Theoretical Estimation

A theoretical estimation of the survival rate was derived by using the degree and the rates of linking nodes as follows. In the case of a node that only has one link we have the following exact relation.

$$P_{s,i} = (1 - f_c) P_{s,j} \tag{11.2}$$

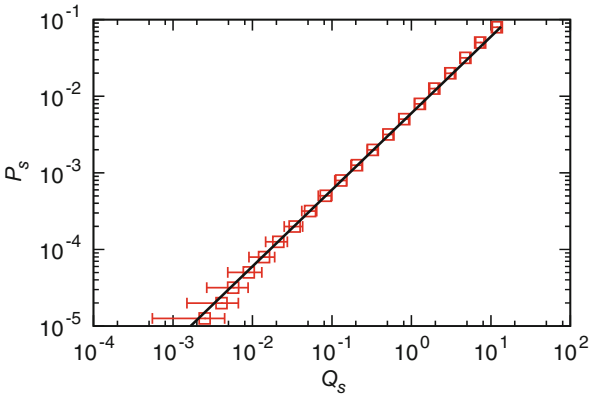

Fig. 11.4 Summation of the survival rate Q_s of nearest-neighbour nodes vs the survival rate P_s. The average is plotted in each log-scaled bin. Error bars are estimated by standard deviation in log-log scale. The line shows Eq. (11.4)

where, the subscript i represents the focusing node, and the subscript j represents the its linking node.

We next extended this formulation to the general case for nodes with multiple links. The probability of the focusing node being connected to the giant component, $P_{s,i}$ is approximated as follows.

$$P_{s,i} = 1 - \prod_{j=1}^{k} \{1 - (1 - f_c) P_{s,j}\} \tag{11.3}$$

On condition that the survival rate P_s is sufficiently small, we can approximate Eq. (11.3) by the following equation.

$$P_{s,i} \simeq (1 - f_c) Q_{s,j} \tag{11.4}$$

Here, $Q_{s,j}$ is defined as $\sum_{j=1}^{k} P_{s,j}$. This equation shows that the survival rate P_s is explained by the summation of the survival rates of linking nodes. In Fig. 11.4, we confirm that this relation is in good agreement. This examination revealed that the survival rate P_s depends on the link number k and the survival rates of the linking nodes, $P_{s,j}$. This result shows that the value $P_{s,i}$ is determined from the global network topology, and that the mean field approach used in Eq. (11.3) works well in deriving Eq. (11.4).

11.5 Network Robustness of Prefectures in Japan

By using the survival rate, we define network robustness of each prefecture as follows. We picked up the top 10,000 ranking nodes (practically consisted of 10,005 nodes counting the same ranking) by the order of survival rates, and counted the number of nodes, and normalised this by the original number of nodes in the extracted network for each prefecture. As shown in Fig. 11.5, Tokyo, Osaka, and seven other prefectures were judged to belong to the most robust class.

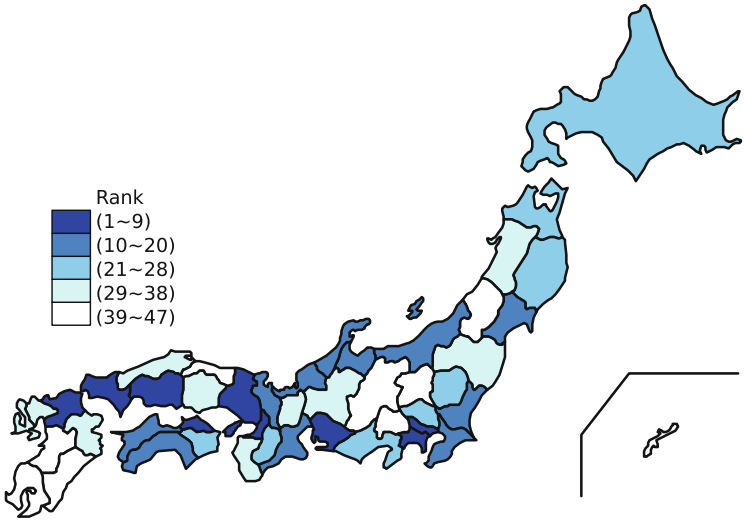

Fig. 11.5 Network robustness for each prefecture in Japan. Here, the network robustness of each prefecture is estimated by the number of top 10,005 robust nodes located in the prefecture divided by the number of nodes of the initially extracted LSCC network in the prefecture. *Colours* show the ranking of network robustness categorised into five classes, (1 ∼ 9), (10 ∼ 20), (21 ∼ 28), (29 ∼ 38), (39 ∼ 47) from the deepest to the lightest

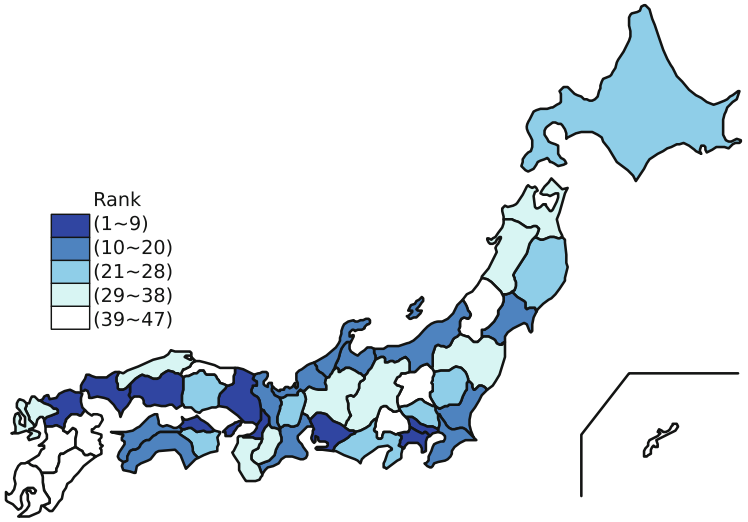

Fig. 11.6 Network robustness for each prefecture with modified normalization. Compared with Fig. 10.5 normalization by the whole number of nodes in the original raw network is applied. *Colours* show the ranking of network robustness categorised into five classes, (1 ∼ 9), (10 ∼ 20), (21 ∼ 28), (29 ∼ 38), (39 ∼ 47) from the deepest to the lightest

As mentioned in Sect. 11.2 we extracted the LSCC from the raw network when we made the percolation simulation. By this operation, the number of nodes was reduced from 612,133 nodes to 327,721 nodes. In order to check this effect, we re-calculated the network robustness normalized by the original number of nodes in the raw network for each prefecture as shown in Fig. 11.6. Comparing with Fig. 11.5, we confirm that changes by this modification are very small, and we find that the eliminated nodes do not affect the results.

11.6 Conclusion

This paper discussed the basic properties of survival rate of a business relation network in Japan based on percolation theory. First, we presented the statistical properties of the survival rate by characterising each node as an index measuring the global network connectivity. Values of survival rate are confirmed to be correlated to network connectivity indices such as degrees or shell numbers. However, as shown in Fig. 11.2, the values distribute widely for the nodes with the same degree number. It is proved in Sect. 11.4.3 that the survival rate of a node is determined by the sum of survival rates of its neighbor nodes. As the survival rates of neighbors are determined by the next neighbors, and so forth, this value reflects information about wider area's network connectivity.

We discussed regional differences from the viewpoint of network robustness. The proposed method enabled us to extract those prefectures that were determined to be robust from the viewpoint of complex network science.

This study involved an examination of the network robustness of a Japanese business relation network in 2011. In future, we plan to analyse the time series variation of network robustness paying attention to local economic activities.

Acknowledgements We would like to express our appreciation to Center for TDB Advanced Data Analysis and Modeling, Tokyo Institute of Technology for providing the datasets. This study is partially supported by the Grant-in-Aid for Scientific Research (C), Grant Number 24540395 and (B), Grant Number 26310207.

References

1. Stauffer D, Aharony A (1994) Introduction to percolation theory. Taylor and Francis, London
2. Last BJ, Thouless DJ (1971) Phys Rev Lett 27:1719
3. Takayasu M, Takayasu, Sato T (1996) Physica A 233:824
4. Barabási AL, Albert R (1999) Science 286:509

5. Watts DJ, Strogatz SH (1998) Nature 393:440
6. Albert R, Jeong H, Barabási AL (2000) Nature 406:378
7. Dorogovtsev SN, Mendes JFF, Samukhin AN (2001) Phys Rev E 64:025101
8. Miura W, Takayasu H, Takayasu M (2012) Phys Rev Lett 108:168701
9. Takayasu M, Sameshima S, Ohnishi T, Ikeda Y, Takayasu H, Watanabe K (2008) Annual Report of the Earth Simulator Center April 2007-March 2008, pp 263–268 http://www.jamstec.go.jp/esc/publication/annual/annual2007/pdf/2project/chapter3/263takayasu.pdf
10. Kitsak M, Gallos LK, Havlin S, Liljeros F, Muchnik L, Stanley HE, Makse HA (2010) Nature Phys 29:1746
11. Kawamoto H, Takayasu H, Jensen HJ, Takayasu M (2015) PLoS ONE 10(4):e0119979. doi: http://dx.doi.org/10.1371/journal.pone.0119979
12. Onnela JP, Saramäki J, Hyvonen J, Szabo G, de Menezes MA, Kaski K, Barabási AL, Kertész J (2007) New J Phys 9:179

Chapter 12
Detectability Threshold of the Spectral Method for Graph Partitioning

Tatsuro Kawamoto and Yoshiyuki Kabashima

Abstract Graph partitioning, or community detection, is an important tool for investigating the structures embedded in real data. The spectral method is a major algorithm for graph partitioning and is also analytically tractable. In order to analyze the performance of the spectral method, we consider a regular graph of two loosely connected clusters, each of which consists of a random graph, i.e., a random graph with a planted partition. Since we focus on the bisection of regular random graphs, whether the unnormalized Laplacian, the normalized Laplacian, or the modularity matrix is used does not make a difference. Using the replica method, which is often used in the field of spin-glass theory, we estimate the so-called detectability threshold; that is, the threshold above which the partition obtained by the method is completely uncorrelated with the planted partition.

12.1 Introduction

Considerable attention has been paid to the graph clustering or community detection problem and a number of formulations and algorithms have been proposed in the literature [1–5]. Although the meaning of a module in each detection method may not be equivalent, we naturally wish to know in what manner the methods perform typically and the point at which a method fails to detect a certain structure in principle [6–8]. Otherwise, we need to test all the existing methods, and this clearly requires a huge cost and is also redundant. Although most studies of the expected performance were experimental, using benchmark testing [9–11], it is expected that theoretical analysis will give us a deeper insight.

As frequently done in benchmarks, we consider random graphs having a planted block structure. The most common model is the so-called stochastic block model (or the planted partition model) [12]. Although many variants of the stochastic block model have been proposed in the literature [13–16], in the simplest case, the

T. Kawamoto (✉) • Y. Kabashima
Tokyo Institute of Technology, Yokohama, Kanagawa, Japan
e-mail: kawamoto@sp.dis.titech.ac.jp; kaba@dis.titech.ac.jp

H. Takayasu et al. (eds.), *Proceedings of the International Conference on Social Modeling and Simulation, plus Econophysics Colloquium 2014*, Springer
Proceedings in Complexity, DOI 10.1007/978-3-319-20591-5_12

vertices within the same module are connected with a high probability p_{in}, while the vertices in different modules are connected with a low probability p_{out}. When the difference between the probabilities is sufficiently large, $p_{in} \gg p_{out}$, the graph has a strong block structure and the spectral method detects almost or exactly the same partition as the planted partition. As we increase the probability between the modules p_{out}, the partition obtained by the spectral method tends to very different from the planted one, and finally, they are completely uncorrelated. The point of the transition is called the *detectability threshold* [17–20]. Since we know that the graph is generated by the stochastic block model, the ultimate limit of this threshold is given by Bayesian inference and it is known that, in the case of the two-block model,

$$c_{\mathrm{in}} - c_{\mathrm{out}} = 2\sqrt{\bar{c}}, \tag{12.1}$$

where $c_{\mathrm{in}} = p_{in}N$, $c_{\mathrm{out}} = p_{out}N$ and $\bar{c}$ is the average degree. N is the total number of vertices in the graph. Equation (12.1) indicates that, even when the vertices are more densely connected within a module than between modules, unless the difference is sufficiently large, it is statistically impossible to infer the embedded structure.

It was predicted by Nadakuditi and Newman in [20] that the spectral method with modularity also has the same detectability threshold as Eq. (12.1). However, it was numerically shown in [21] that this applies only to the case where the graph is not sparse. Despite its significance, a precise estimate of the detectability threshold of the spectral method in the sparse case seems to remain missing.

In this article, we derive an estimate of the detectability threshold of the spectral method of the two-block regular random graph. It should be noted that the simplest stochastic block model, which we explained above, has Poisson degree distribution, while we impose a constraint such that the degree does not fluctuate. Therefore, our results do not directly provide an answer to the missing part of the problem. They do, however, provide a fruitful insight into the performance of the spectral method. Moreover, in the present situation, we do not face the second difficulty of the spectral method: the localization of the eigenvectors. Although the localization of eigenvectors is another important factor in the detectability problem, it is outside the scope of this article.

This article is organized as follows. In Sect. 12.2, we briefly introduce spectral partitioning of two-block regular random graphs and mention that the eigenvector corresponding to the second-smallest eigenvalue contains the information of the modules. In Sect. 12.3, we show the average behavior of the second-smallest eigenvalue and the corresponding eigenvector as a function of the parameters in the model. Finally, Sect. 12.4 is devoted to the conclusion.

12.2 Spectral Partitioning of Regular Random Graphs With Two-Block Structure

The model parameters in the two-block regular random graph are the total number of vertices N, the degree of each vertex c, and the fraction of the edges between modules $\gamma = l_{\text{int}}/N$. The graph is constructed as follows. We first set module indices on the vertices, each of which has c half edges, or stubs, and randomly connect the vertices in different modules with l_{int} edges. We connect the rest of the edges at random within the same module. We repeat the process so that every edge is connected to a pair of vertices. This random graph is sparse when $c = O(1)$, because the number of edges is of the same order as the number of vertices N. We calculate the degree of correlation between the partition obtained by the spectral method and the planted partition as γ varies.

The choices of the matrix that can be used in the spectral method is wide. The popular matrices are the unnormalized Laplacian L, the normalized Laplacian $\mathscr{L}$, and the modularity matrix B. For the bisection of regular random graphs, however, all the partitions they yield have shown to be the same [22]. Thus, we analyze the unnormalized Laplacian L, since it is the simplest. The basic procedure of the spectral bisection with the unnormalized Laplacian L is quite simple. We solve for the eigenvector corresponding to the second-smallest eigenvalue of L and classify each vertex according to the sign of the corresponding component of the eigenvector; the vertices with the same sign belong to the same module. Therefore, our goal is to calculate the behavior of the sign of the eigenvector as a function of γ.

12.3 Detectability Threshold

We use the so-called replica method, which is often used in the field of spin-glass theory in statistical physics. The basic methodology here is parallel to that in [23]. Although the final goal is to solve for the eigenvector corresponding to the second-smallest eigenvalue or the statistics of its components, let us consider estimating the second-smallest eigenvalue, averaged over the realization of the random graphs. We denote by $[\dots]_L$ the random average over the unnormalized Laplacians of the possible graphs. For this purpose, we introduce the following "Hamiltonian" $H(\boldsymbol{x}|L)$, "partition function" $Z(\beta|L)$, and "free energy density" $f(\beta|L)$:

$$H(\boldsymbol{x}|L) = \frac{1}{2}\boldsymbol{x}^{\mathrm{T}} L \boldsymbol{x}, \tag{12.2}$$

$$Z(\beta|L) = \int d\boldsymbol{x}\, \mathrm{e}^{-\beta H(\boldsymbol{x}|L)} \delta(|\boldsymbol{x}|^2 - N)\delta(\mathbf{1}^{\mathrm{T}}\boldsymbol{x}), \tag{12.3}$$

$$f(\beta|L) = -\frac{1}{N\beta} \ln Z(\beta|L), \tag{12.4}$$

where $\boldsymbol{x}$ is an N-dimensional vector, $\mathbf{1}$ is a vector in which each element equals one, and T represents the transpose. The delta function $\delta(|\boldsymbol{x}|^2 - N)$ in (12.3) is to impose the norm constraint. It should be noted that the eigenvector corresponding to the smallest eigenvalue is proportional to $\mathbf{1}$ and this choice is excluded by the constraint $\delta(\mathbf{1}^{\mathrm{T}}\boldsymbol{x})$. In the limit of $\beta \to \infty$, in conjunction with the operation of $\delta(\mathbf{1}^{\mathrm{T}}\boldsymbol{x})$, the contribution in the integral of the "partition function" $Z(\beta|L)$ is dominated by the vector that minimizes the value of the "Hamiltonian" $H(\boldsymbol{x}|L)$, under the constraint of being orthogonal to the eigenvector $\mathbf{1}$ of the smallest eigenvalue. Therefore, the "partition function" is dominated by the eigenvector of the second-smallest eigenvalue and the "free energy density" $f(\beta|L)$ extracts it, i.e.,

$$\lambda_2 = 2 \lim_{\beta\to\infty} f(\beta|L). \tag{12.5}$$

The quantity we need is $[\lambda_2]_L$, the second-smallest eigenvalue averaged over the unnormalized Laplacians. However, because the average of the logarithm of the "partition function" is difficult to calculate, we recast $[\lambda_2]_L$ as

$$\begin{aligned}[\lambda_2]_L &= -2 \lim_{\beta\to\infty} \frac{1}{N\beta} [\ln Z(\beta|L)]_L \\ &= -2 \lim_{\beta\to\infty} \lim_{n\to 0} \frac{1}{N\beta} \frac{\partial}{\partial n} \ln [Z^n(\beta|L)]_L \,. \end{aligned} \tag{12.6}$$

The assessment of $[Z^n(\beta|L)]_L$ is also difficult for a general real number n. However, when n takes positive integer values, $[Z^n(\beta|L)]_L$ can be evaluated as follows. For a positive integer n, $[Z^n(\beta|L)]_L$ is expressed as

$$\begin{aligned}[Z^n(\beta|L)]_L &= \int \left(\prod_{a=1}^{n} d\boldsymbol{x}_a \delta(|\boldsymbol{x}_a|^2 - N) \delta(\mathbf{1}^{\mathrm{T}}\boldsymbol{x}_a) \right) \left[\exp\left(-\frac{\beta}{2} \sum_a \boldsymbol{x}_a^{\mathrm{T}} L \boldsymbol{x}_a \right) \right]_L \\ &\equiv \int \left(\prod_{a=1}^{n} d\boldsymbol{x}_a \delta(|\boldsymbol{x}_a|^2 - N) \delta(\mathbf{1}^{\mathrm{T}}\boldsymbol{x}_a) \right) \exp\left(H_{\mathrm{eff}}(\beta, \boldsymbol{x}_1, \boldsymbol{x}_2, \ldots, \boldsymbol{x}_n) \right) . \end{aligned} \tag{12.7}$$

This means that $[Z^n(\beta|L)]_L$ has a meaning of a partition function for a system of n-replicated variables $\boldsymbol{x}_1, \boldsymbol{x}_2, \ldots, \boldsymbol{x}_n$ that is subject to no quenched randomness. In addition, the assumption of the graph generation guarantees that the effective Hamiltonian $\mathscr{H}_{\mathrm{eff}}(\beta, \boldsymbol{x}_1, \boldsymbol{x}_2, \ldots, \boldsymbol{x}_n)$ is of the mean field type. These indicate that $N^{-1} \ln [Z^n(\beta|L)]_L$ for $n = 1, 2, \ldots$ can be evaluated exactly by the saddle point method with respect to certain macroscopic variables (order parameters) as $N \to \infty$. After some calculations, we indeed reach an expression with the saddle point

evaluation as

$$\frac{1}{N}\ln[Z^n(\beta|L)]_L = \underset{\{Q_r\},\{\hat{Q}_r\},\{\phi_a\},\{\psi_a\},\eta}{\text{extr}} \left\{ NK_{\text{I}}(Q_r,\hat{Q}_r) + \frac{\beta}{2}\sum_a \phi_a - \sum_{r=1,2} K_{\text{II}r}(Q_r,\hat{Q}_r) + \frac{1}{N}\sum_{r=1,2} \ln K_{\text{III},r}(\hat{Q}_r,\{\phi_a\},\{\psi_a\}) + \eta\gamma - \frac{1}{N}\ln \mathscr{N}_G - \ln c! \right\}, \tag{12.8}$$

where $\mathscr{N}_G$ is the total number of graph configurations and

$$\begin{aligned} K_{\text{I}}(Q_r,\hat{Q}_r) &= \sum_{r,s=1,2} \frac{p_r p_s}{2} \int d\boldsymbol{\mu}^{(r)} d\boldsymbol{\nu}^{(s)}\, Q_r(\boldsymbol{\mu}^{(r)}) Q_s(\boldsymbol{\nu}^{(s)}) \\ &\quad \times \mathrm{e}^{-(1-\delta_{rs})\eta - \frac{\beta}{2}\sum_a (\mu_a^{(r)} - \nu_a^{(s)})^2}, \\ K_{\text{II}r}(Q_r,\hat{Q}_r) &= p_r \int d\boldsymbol{\mu}^{(r)}\, \hat{Q}_r(\boldsymbol{\mu}^{(r)}) Q_r(\boldsymbol{\mu}^{(r)}), \\ K_{\text{III}r}(\hat{Q}_r,\{\phi_a\},\{\psi_a\}) &= \int \prod_{i\in V_r}\prod_{a=1}^{n} dx_{ia} \\ &\quad \times \prod_{i\in V_r} \left(\hat{Q}_r^c(\boldsymbol{x}_i) \exp\left[-\frac{\beta}{2}\sum_a \left(\phi_a x_{ia}^2 + \psi_a x_{ia} \right) \right] \right). \end{aligned} \tag{12.9}$$

In the above equations, four functions $Q_r(\mu_1^{(r)},\ldots,\mu_n^{(r)})$ and $\hat{Q}_r(\mu_1^{(r)},\ldots,\mu_n^{(r)})$ $(r = 1, 2)$ play the roles of order parameters.

Unfortunately, this expression cannot be employed directly for the computation of (6) as $Q_r(\mu_1^{(r)},\ldots,\mu_n^{(r)})$ and $\hat{Q}_r(\mu_1^{(r)},\ldots,\mu_n^{(r)})$ are defined only for $n = 1, 2, \ldots$. To overcome this inconvenience, we introduce the following assumption at the dominant saddle point.

> [Replica symmetric assumption] The right hand side of (12.7) is invariant under any permutation of replica indices $a = 1, 2, \ldots, n$. We assume that this property, which is termed the *replica symmetry*, is also owned by the dominant saddle point of (12.8).

In the current system, this restricts the functional forms of $Q_r(\mu_1^{(r)},\ldots,\mu_n^{(r)})$ and $\hat{Q}_r(\mu_1^{(r)},\ldots,\mu_n^{(r)})$ as

$$\begin{aligned} Q_r(\mu_1,\ldots,\mu_n) &= \left(\frac{cp_r - \gamma}{Np_r^2} \right)^{1/2} \int dA dH\, q_r(A,H) \left(\frac{\beta A}{2\pi} \right)^{\frac{n}{2}} \\ &\quad \times \exp\left[-\frac{\beta A}{2} \sum_{a=1}^{n} \left(\mu_a - \frac{H}{A} \right)^2 \right], \end{aligned}$$

$$\hat{Q}_r(\mu_1,\ldots,\mu_n) = c\left(\frac{cp_r-\gamma}{Np_r^2}\right)^{-1/2}\int d\hat{A}d\hat{H}\,\hat{q}_r(\hat{A},\hat{H}) \times \exp\left[\frac{\beta}{2}\sum_{a=1}^{n}\left(\hat{A}\mu_a^2+2\hat{H}\mu_a\right)\right], \tag{12.10}$$

which yields an expression of $N^{-1}\ln[Z^n(\beta|L)]_L$ that can be extended for n of a real number. We then substitute that expression into (12.6), which finally provides

$$\begin{aligned}[\lambda_2]_L = -\underset{\{q_r\},\{\hat{q}_r\},\phi,\psi}{\mathrm{extr}}\Bigg\{&\int dAdH\int dA'dH'\,\Xi(A,H,A',H')\\ &\times\frac{cp_1p_2}{2}\Bigg(\left(\frac{p_1}{p_2}+\Gamma\right)q_1(A,H)q_1(A',H')\\ &+\left(\frac{p_2}{p_1}+\Gamma\right)q_2(A,H)q_2(A',H')\\ &+2\left(1-\Gamma\right)q_1(A,H)q_2(A',H')\Bigg)\\ &+\phi\\ &-c\sum_{r=1,2}p_r\int dAdH\int d\hat{A}d\hat{H}\,q_r(A,H)\hat{q}_r(\hat{A},\hat{H})\left(\frac{(H+\hat{H})^2}{A-\hat{A}}-\frac{H^2}{A}\right)\\ &+\sum_{r=1,2}p_r\int\prod_{g=1}^{c}\left(d\hat{A}_g d\hat{H}_g\hat{q}_r(\hat{A}_g,\hat{H}_g)\right)\frac{\left(\psi/2-\sum_g\hat{H}_g\right)^2}{\phi-\sum_g\hat{A}_g}\Bigg\}, \end{aligned}\tag{12.11}$$

where we set

$$\Gamma = 1-\frac{\gamma}{cp_1p_2}, \tag{12.12}$$

$$\Xi(A,H,A',H') = \frac{(1+A')H^2+(1+A)H'^2+2HH'}{(1+A)(1+A')-1}-\frac{H^2}{A}-\frac{H'^2}{A'}. \tag{12.13}$$

The above procedure is often termed the *replica method*. Although its mathematical validity of the replica method has not yet been proved, we see that our assessment based on the simplest permutation symmetry for the replica indices offers a fairly accurate prediction for the experimental results below.

Due to the space limitation, we hereafter show only the results, omitting all the details of the calculation (see [24] for complete calculation including detailed

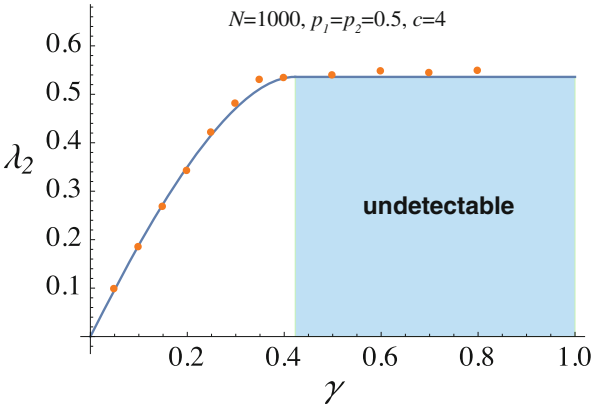

Fig. 12.1 Second-smallest eigenvalue as a function of γ. The solid line represents the estimate of the average over the realization of the graphs $[\lambda_2]_L$ and the dots represent the results of the numerical experiment of a single realization with $N = 1000$ and $c = 4$. The module sizes are set to be equal, $p_1 = p_2 = 0.5$.

derivation of (12.11)). In the limit of large size $N \to \infty$, the saddle-point analysis of (12.11) yields the solution

$$[\lambda_2]_L = \begin{cases} (1-\Gamma)\left(c-1-\frac{1}{\Gamma}\right) & (1/\sqrt{c-1} \le \Gamma), \\ c - 2\sqrt{c-1} & \text{otherwise}, \end{cases} \tag{12.14}$$

where $\Gamma = 1 - \gamma/(cp_1p_2)$; we set the size of each module as $N_1 = p_1N$ and $N_2 = p_2N$. The region of constant eigenvalue in (12.14) indicates that the second-smallest eigenvalue is in the spectral band, i.e., the information of the modules is lost there and an undetectable region exists. Therefore, the boundary of (12.14) is the critical point where the phase transition occurs. The plot of the second-smallest eigenvalue $[\lambda_2]_L$ is shown in Fig. 12.1. Although the dots represent the results of the numerical experiment of a single realization, the results agree with (12.14) quite well.

In terms of γ, the boundary of Eq. (12.14) can be recast as

$$\gamma = cf(c)p_1p_2, \tag{12.15}$$

where

$$f(c) = 1 - \frac{1}{\sqrt{c-1}}. \tag{12.16}$$

Since cp_1p_2 is the value of γ in a uniform (i.e., one-block) regular random graph, the factor $f(c)$ represents the low value of the threshold as compared to that in the uniform random case.

The distribution of the components of the corresponding eigenvector can also be obtained through this calculation. Although it cannot be written analytically, we can solve for it by iterating a set of integral equations that result from the saddle-point evaluation of the right hand side of (12.6). As shown in Fig. 12.2, the results

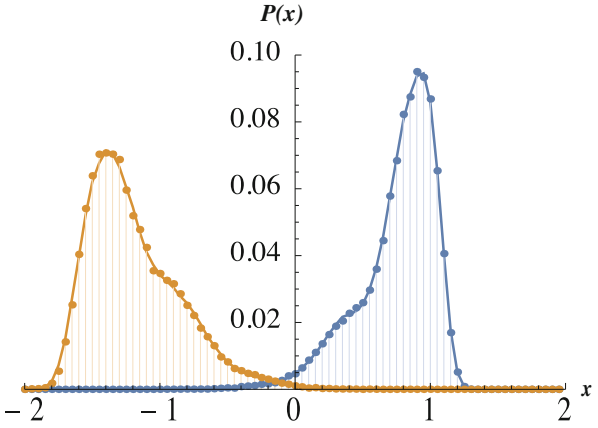

Fig. 12.2 Distributions of the elements in the eigenvector corresponding to the second-smallest eigenvector. Each plot shows the distribution of elements in each module, i.e., the distribution on the left corresponds to the module that is supposed to have negative sign elements and the distribution on the right corresponds to the module that is supposed to have positive sign elements, respectively. The *dots* represent the average results of the numerical experiments, taken over 100 samples. The ratio of the modules are set to be $p_1 = 0.6$ and $p_2 = 0.4$

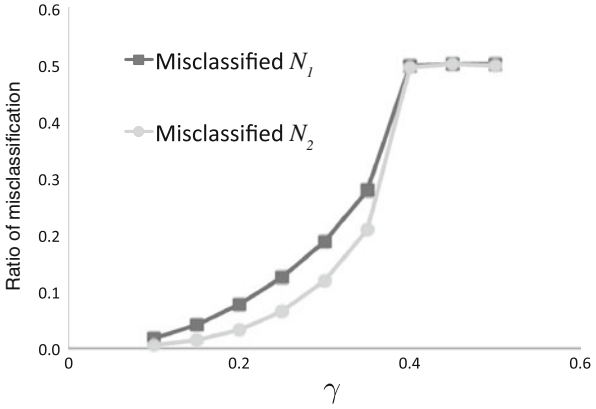

Fig. 12.3 Fraction of misclassified vertices in each module. As the parameter γ increases, the number of misclassified vertices increases polynomially

of our analysis agree with the corresponding numerical experiment excellently. In Fig. 12.2, the dots represent the average over 100 realizations of the random graphs. The ratio of misclassified vertices are shown in Fig. 12.3. It increases polynomially with respect to γ and saturates at the detectability threshold.

It should be note that, even when the number of vertices is infinity, the fraction of misclassified vertices remains finite. The misclassification of the vertices occurs because the planted partition is not the optimum in the sense of the spectral bisection. The spectral method with the unnormalized Laplacian L constitute

the continuous relaxation of the discrete minimization problem of the so-called *RatioCut*. The RatioCut is lower for a partition with a sparse cut, while it penalizes for unbalanced partitions in the sense of the number of the vertices within a module; there may always exist a better cut in the sense of the RatioCut than the planted partition in the graph when γ is large.

Finally, let us compare our estimate with results of studies in the literature. In the following, we focus on the case of equal size modules, i.e., $p_1 = p_2 = 0.5$. Let the total degree within a module be $K_{\rm in}$ and let the total degree from one module to the others be $K_{\rm out}$. Since we have $K = cN = 2(K_{\rm in} + K_{\rm out})$ and $K_{\rm out} = \gamma N$, Eq. (12.15) reads

$$K_{\rm in} - K_{\rm out} = \frac{N}{2}\frac{c}{\sqrt{c-1}}. \tag{12.17}$$

In addition, in the limit $N \to \infty$, we have

$$K_{\rm in} = \frac{N^2}{4}p_{\rm in} = \frac{N}{4}c_{\rm in}, \tag{12.18}$$

$$K_{\rm out} = \frac{N^2}{4}p_{\rm out} = \frac{N}{4}c_{\rm out}. \tag{12.19}$$

Therefore, (12.17) can be recast as

$$c_{\rm in} - c_{\rm out} = 2\frac{c}{\sqrt{c-1}}. \tag{12.20}$$

This condition converges to the ultimate detectability threshold (12.1) in the dense limit $c \to \infty$. There exists, however, a huge gap between (12.1) and (12.20) when the degree c is small; considering the fact that the upper bound of the parameter $c_{\rm in} - c_{\rm out}$ is $2c$, this gap is not negligible at all. Thus, the implication of our results is that we cannot expect the spectral threshold to detect modules all the way down to the ultimate detectability threshold, even in regular random graphs, where the localization of the eigenvectors is absent.

12.4 Conclusion

In summary, we derived an estimate of the detectability threshold (12.20) of the spectral method of the two-block regular random graphs. The threshold we obtained agrees with the results of the numerical experiment excellently and is expected to be asymptotically exact in the limit $N \to \infty$. Our results indicate that the spectral method cannot detect modules all the way down to the ultimate detectability threshold (12.1), even when the degree is fixed to a constant. Since the threshold (12.20) converges to (12.1) as the degree c increases, this gap becomes

negligible in the case where the degree is sufficiently large and this supports the results obtained by Nadakuditi and Newman [20].

A method for achieving the ultimate detectability threshold with the spectral method has already been proposed by Krzakala et al. [25]. They proposed using a matrix called the non-backtracking matrix, which avoids the elements of eigenvectors to be localized at a few vertices. A question about this formalism is: to what extent is the gap in the detectability in fact closed by the non-backtracking matrix as compared to the Laplacians? Our estimate gives a clue to the answer to this question. In order to gain further insight, we need to analyze the case of graphs with degree fluctuation. In that case, the methods using the unnormalized Laplacian and the normalized Laplacian will no longer be equivalent. Moreover, it is important to verify the effect of the localization of eigenvectors on the detectability. These problems remain as future work.

Acknowledgements This work was supported by JSPS KAKENHI Nos. 26011023 (TK), 25120013 (YK), and the JSPS Core-to-Core Program "Non-equilibrium dynamics of soft matter and information."

References

1. Fortunato S (2010) Phys Rep 486:75
2. Luxburg U (2007) Stat Comput 17(4):395
3. Newman MEJ (2006) Phys Rev E 74(3):036104
4. Rosvall M, Bergstrom C (2008) Proc Natl Acad Sci USA 105(4):1118
5. Palla G, Derényi I, Farkas I, Vicsek T (2005) Nature 435(7043):814
6. Fortunato S, Barthélemy M (2007) Proc Natl Acad Sci USA 104(1):36
7. Good BH, de Montjoye YA, Clauset A (2010) Phys Rev E 81(4):046106
8. Kawamoto T, Rosvall M (2015) Phys Rev E 91:012809
9. Leskovec J, Lang KJ, Anirban D, Mahoney MW (2009) Internet Math 6(1):29
10. Lancichinetti A, Fortunato S (2009) Phys Rev E 80(5), 056117
11. Aldecoa R, Marín I (2013) Sci Rep 3:2216
12. Holland PW, Laskey KB, Leinhardt S (1983) Soc Networks 5(2):109
13. Airoldi EM, Blei DM, Fienberg SE, Xing EP (2008) J Mach Learn Res 9:1981
14. Karrer B, Newman MEJ (2011) Phys Rev E 83(1):016107
15. Ball B, Karrer B, Newman MEJ (2011) Phys Rev E 84(3):036103
16. Peixoto TP (2012) Phys Rev E 85(5):056122
17. Reichardt J, Leone M (2008) Phys Rev Lett 101(7):078701
18. Decelle A, Krzakala F, Moore C, Zdeborová L (2011) Phys Rev Lett 107(6):065701
19. Decelle A, Krzakala F, Moore C, Zdeborová L (2011) Phys Rev E 84(6):066106
20. Nadakuditi RR, Newman MEJ (2012) Phys Rev Lett 108(18):188701
21. Zhang P, Krzakala F, Reichardt J, Zdeborová L (2012) J Stat Mech 2012(12):P12021
22. Newman MEJ (2013) Phys Rev E 88(4):042822

23. Kabashima Y, Takahashi H (2012) J Phys A 45(32):325001
24. Kawamoto T, Kabashima Y (2015) Limitations in the spectral method for graph partitioning: Detectability threshold and localization of eigenvectors. Phys Rev E 91(062):803 doi:10.1103/PhysRevE.91.062803
25. Krzakala F, Moore C, Mossel E, Neeman J, Sly A, Zdeborová L, Zhang P (2013) Proc Natl Acad Sci USA 110(52):20935

Chapter 13
Spread of Infectious Diseases with a Latent Period

Kanako Mizuno and Kazue Kudo

Abstract Infectious diseases spread through human networks. Susceptible-Infected-Removed (SIR) model is one of the epidemic models to describe infection dynamics on a complex network connecting individuals. In the metapopulation SIR model, each node represents a population (group) which has many individuals. In this paper, we propose a modified metapopulation SIR model in which a latent period is taken into account. We call it SIIR model. We divide the infection period into two stages: an infected stage, which is the same as the previous model, and a seriously ill stage, in which individuals are infected and cannot move to the other populations. The two infectious stages in our modified metapopulation SIR model produce a discontinuous final size distribution. Individuals in the infected stage spread the disease like individuals in the seriously ill stage and never recover directly, which makes an effective recovery rate smaller than the given recovery rate.

13.1 Introduction

Infectious diseases spread through human networks. Susceptible-Infected-Removed (SIR) model is one of the epidemic models to describe infection dynamics on a complex network connecting individuals. The ratio of the transmission rate to the recovery rate is called the basic reproduction number R_0. It is the expected number of infections caused by a typical infectious individual in a completely susceptible population [1, 2]. In the standard SIR model, the outbreak occurs when $R_0 > 1$. The likely magnitude of the outbreak, which is called the expected final size of the epidemic, depends only on R_0 [2, 3].

The spread of infectious diseases also depends on human mobility. In metapopulation SIR models, movements between different populations (groups) are taken into account [4–6]. Each node of the metapopulation network represents a group

K. Mizuno • K. Kudo (✉)
Department of Computer Science, Ochanomizu University, Tokyo, Japan
e-mail: mizuno.kanako@is.ocha.ac.jp; kudo@is.ocha.ac.jp

H. Takayasu et al. (eds.), *Proceedings of the International Conference on Social Modeling and Simulation, plus Econophysics Colloquium 2014*, Springer Proceedings in Complexity, DOI 10.1007/978-3-319-20591-5_13

of individuals. Individuals can move between two nodes connected by a link. Although the epidemic threshold is R_0 in each group, the global invasion threshold in the metapopulation system depends on the mobility rate as well as its network structure [5, 6].

In this paper, we propose a modified metapopulation SIR model in which a latent period is taken into account. Infected individuals behave like susceptible ones when they do not feel sick. They move between linked populations and spread diseases across different populations. We consider that such infected individuals are in a latent period. We assume that infected individuals become too sick to move after the latent period. Such ill individuals infect only the susceptible ones in the same population. This model is different from the SEIR model [7], which is a common epidemic model in which a latent period is incorporated as an "Exposed" state. However, it belongs to a family of generalized SIR models that include multiple infectious stages [2]. The two infectious stages in our modified metapopulation SIR model produce a discontinuous final size distribution with a jump at $R_0 = 1$.

The rest of the paper is organized as follows. The metapopulation SIR model and the modified SIR model are introduced in Sect. 13.2. We demonstrate the discontinuous final size distribution of the modified model in Sect. 13.3. The effective recovery rate, which is different from the given recovery rate, is estimated, and it is the key to find what causes the discontinuity. Discussions and conclusions are given in Sect. 13.4.

13.2 Model

First we introduce a metapopulation SIR model, which is an SIR model that is extended to metapopulation networks. In the metapopulation SIR model, each node represents a population (group) which has many individuals, and each individual is in one of three states: S (susceptible), I (infected) or R (recovered). Individuals of state S are infected by those of state I in the same population. The infection rate is given by $\alpha I_m/N_m$, where $N_m = S_m + I_m + R_m$ with S_m, I_m, and R_m being the number of susceptible, infected, and recovered individuals of population m, respectively. In other words, the rate that S becomes I depends on the transmission rate α and the proportion of I in the same population. The constant rate that I becomes R, i.e., recovery rate, is defined as β. We here assume that all individuals move between the populations connected with links in the network at a constant rate w. The travel rate

w is the same for all the individuals. The time evolution of the numbers of S, I and R in each population is described by

$$\partial_t S_n = -\alpha S_n I_n / N_n + w \sum_m (S_m - S_n), \tag{13.1a}$$

$$\partial_t I_n = \alpha S_n I_n / N_n - \beta I_n + w \sum_m (I_m - I_n), \tag{13.1b}$$

$$\partial_t R_n = \beta I_n + w \sum_m (R_m - R_n), \tag{13.1c}$$

where the summations are taken over all the populations connected with population n.

Next, we divide the infection period into two stages: an infected stage, which is the same as the previous model, and a seriously ill stage, in which individuals are infected and cannot move to the other populations. We call this model SIIR model. In this model, each individual is in one state of S (susceptible), H (infected), I (seriously ill), and R (recovered). Individuals of S in population m are infected and become H at rate $\alpha(H_m + I_m)/N_m$, where $N_m = S_m + H_m + I_m + R_m$. Individuals of H become I at a constant rate μ. Individuals of I recover and become R at a rate β. In the SIIR model, individuals of H move between the populations connected with links at a rate w, however, individuals of I do not. The time evolution of the numbers of S, H, I and R in each population is described by

$$\partial_t S_n = -\alpha S_n (H_n + I_n)/N_n + w \sum_m (S_m - S_n), \tag{13.2a}$$

$$\partial_t H_n = \alpha S_n (H_n + I_n)/N_n - \mu H_n + w \sum_m (H_m - H_n), \tag{13.2b}$$

$$\partial_t I_n = \mu H_n - \beta I_n, \tag{13.2c}$$

$$\partial_t R_n = \beta I_n + w \sum_m (R_m - R_n), \tag{13.2d}$$

where the summations are taken over all the populations connected with population n.

13.3 Final Size Distribution

The spread of a disease is expressed by attack ratio, which is the final proportion of R when I disappears in the entire metapopulation. The attack ratio plotted as the function of the basic reproduction number α/β is called a final size distribution. The final size distributions of the SIR model and SIIR models are shown in Fig. 13.1. In

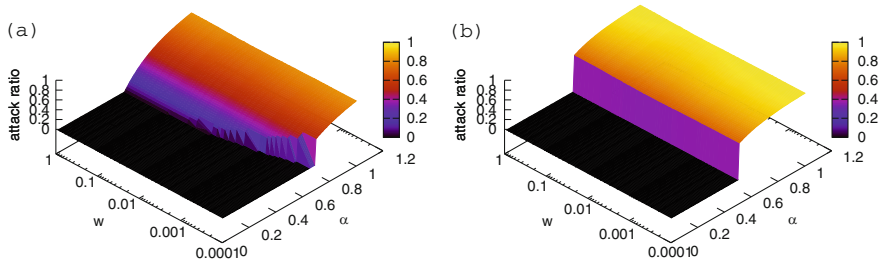

Fig. 13.1 Final size distributions of (**a**) metapopulation SIR model and (**b**) metapopulation SIIR model as the function of the transmission rate α and the travel rate w. In both cases, the recovery rate is $\beta = 0.5$

this simulation, the number of individuals in each state is taken as a real number and the time step is discrete. We use a scale-free network with 900 nodes, whose degree distribution is $P(k) \sim k^{-\gamma}$ with $\gamma = 2.5$. The essential results do not depend on γ. In the initial state, 100 susceptible individuals belong to each node except for one randomly selected node in which one infected individual is included. The global invasion does not occur when $\alpha < \beta$ in the SIIR model as well as the SIR model. The change in attack ratio is continuous at $\alpha = \beta$ in the high-w region in the SIR model, however, it is discontinuous in all region in the SIIR model. The shift of threshold in the low-w regions of the SIR model is often observed in metapopulation networks [5, 6].

In this paper, we focus on the discontinuous final size distribution of the SIIR model. The jump in the attack ratio arises from the difference between the given recovery rate and an effective recovery rate. In the SIIR model, individuals H spread the disease like individuals I and never become R directly. Therefore, the effective recovery rate β' is expected to be smaller than the given recovery rate β.

We show how to evaluate β' below. Disregarding traveling between populations, the SIIR model (13.2) is rewritten as

$$\partial_t S = -\alpha S(H + I), \tag{13.3a}$$

$$\partial_t H = \alpha S(H + I) - \mu H, \tag{13.3b}$$

$$\partial_t I = \mu H - \beta I, \tag{13.3c}$$

$$\partial_t R = \beta I, \tag{13.3d}$$

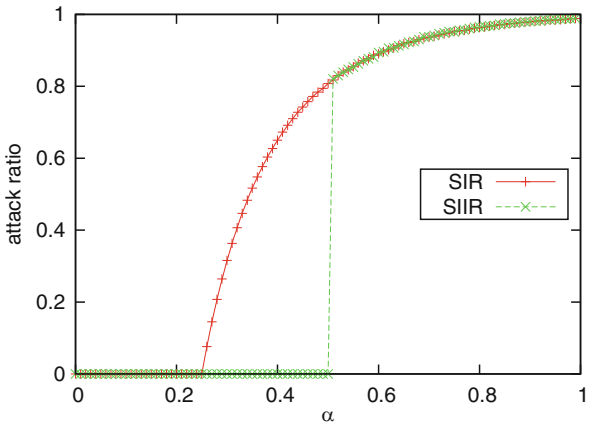

Fig. 13.2 The final size distribution as the function of the transmission rate α for the SIR model with the given recovery rate $\beta = 0.25$ is compared with that for the SIIR model with the effective recovery rate $\beta' = 0.25$, which is calculated from Eq. (13.4) with $\beta = 0.5$ and $\mu = 0.5$. Both curves agree in the region where $\alpha > 0.5$. The travel rate $w = 0.1$ for both curves

where $S = S_n/N_n, H = H_n/N_n, I = I_n/N_n$ and $R = R_n/N_n$. Combining Eqs. (13.3b) and (13.3c), we have

$$\partial_t(H + I) = \alpha S(H + I) - \beta'(H + I),$$
$$\beta' = \frac{I}{H + I}\beta.$$

We here take $\partial_t I = 0$, which leads to $H = (\beta/\mu)I$. Then, the effective recovery rate is calculated as

$$\beta' = \frac{\mu}{\beta + \mu}\beta. \tag{13.4}$$

Figure 13.2 illustrates that the evaluation of the effective recovery rate is appropriate. The simulation is performed in the same network with the same initial condition as Fig. 13.1. The travel rate is $w = 0.1$, which is in the high-w region. The attack ratio for the SIIR model is calculated for $\beta = 0.5$ and $\mu = 0.5$. In this case, the effective recovery rate is $\beta' = 0.25$. The final size distribution for the SIR model with the given recovery rate $\beta = 0.25$ agrees with that for the SIIR model in the region where $\alpha > 0.5$. This result implies the following. The effective recovery rate in the SIIR model is given by β', however, global invasion cannot occur when $\alpha < \beta$. The difference between β and β' causes the discontinuous final size distribution of the SIIR model.

Since we disregarded traveling between populations when we evaluate the effective recovery rate, the assumption that I is immobile should be irrelevant to the discontinuity in the final size distribution of the SIIR model. We now modify the SIIR model (13.2), replacing Eq. (13.2c) by

$$\partial_t I_n = \mu H_n - \beta I_n + w\sum_m (I_m - I_n). \tag{13.5}$$

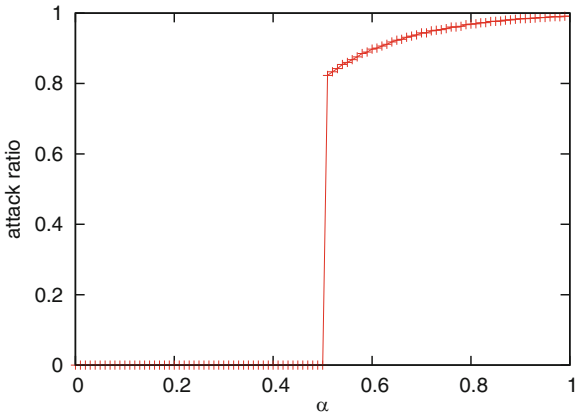

Fig. 13.3 The final size distribution of the modified SIIR model in which H moves between populations. α is the transmission rate. The travel rate $w = 0.1$

Figure 13.3 shows the final size distribution of the modified SIIR model. The simulation is performed in the same conditions as Fig. 13.2. The profile of the SIIR curve in Fig. 13.2 looks the same as the curve in Fig. 13.3. Therefore, the cause of the discontinuous final size distribution is the division of the infection period into two stages, and the mobility of I has no effect on the discontinuity.

13.4 Discussions and Conclusions

The effective recovery rate β', which is given by Eq. (13.4), can be evaluated by another way. The basic reproduction number for the generalized SIR model that includes n infectious stages is given by

$$R_0 = \sum_{i=1}^{n} \frac{\alpha_i}{\beta_i}, \tag{13.6}$$

where α_i is the transmission rate of the ith infectious stage, and $1/\beta_i$ is the mean duration of the stage [2, 8]. In our SIIR model, $\alpha_1 = \alpha_2 = \alpha$, $\beta_1 = \mu$ and $\beta_2 = \beta$, and thus, $R_0 = \alpha/\mu + \alpha/\beta = \alpha(\mu + \beta)/(\mu\beta)$. Therefore,

$$\beta' = \frac{\alpha}{R_0} = \frac{\mu\beta}{\mu + \beta}, \tag{13.7}$$

which is the same as Eq. (13.4).

In conclusion, the discontinuous final size distribution in the SIIR model is caused by the division of the infection period into two stages and the fact that the global invasion cannot occur when $\alpha < \beta$. The final size distribution depends on the

effective recovery rate β', and its shape coincides with that of the SIR model with a recovery rate $\beta = \beta'$ in the region where $\alpha > \beta$.

Acknowledgements We would like to thank H. Takayasu and H. Nishiura for valuable suggestions and comments.

References

1. Anderson RM, May RM (1991) Infectious diseases of humans: dynamics and control. Oxford University Press, Oxford
2. Ma J, Earn DJD (2006) Bull Math Biol 68:679
3. Anderson D, Watson R (1980) Biometrika 67:191
4. Keeling MJ, Rohani P (2002) Ecol Lett 5:20
5. Cross PC, Lloyd-Smith JO, Johnson PLF, Getz WM (2005) Ecol Lett 8:587
6. Colizza V, Vespignani A (2007) Phys Rev Lett 99:148701
7. Schwartz I, Smith H (1983) J Math Biol 18:233
8. Hyman JM, Li J, Stanley EA (1999) Math Biosci 155:77